Microporous and Mesoporous Materials 276 (2019) 213–222

Contents lists available at ScienceDirect

Microporous and Mesoporous Materials

journal homepage: www.elsevier.com/locate/micromeso

Preparation of benzodiimidazole-containing covalent triazine frameworks for enhanced selective CO_2 capture and separation

Jianfeng Du[a], Yuanzheng Cui[a], Yuchuan Liu[a], Rajamani Krishna[c], Yue Yu[a], Shun Wang[a], Chenghui Zhang[a], Xiaowei Song[a,*], Zhiqiang Liang[a,b,**]

[a] State Key Lab of Inorganic Synthesis and Preparative Chemistry, Jilin University, Changchun, 130012, PR China
[b] Key Laboratory of Advanced Materials of Tropical Island Resources, Ministry of Education, College of Materials and Chemical Engineering, Hainan University, PR China
[c] Van 't Hoff Institute for Molecular Sciences, University of Amsterdam, Science Park 904, 1098 XH, Amsterdam, the Netherlands

ARTICLE INFO

Keywords:
Covalent triazine frameworks
Benzodiimidazole
CO_2 adsorption
Gas separation

ABSTRACT

Covalent triazine frameworks (CTFs) were frequently prepared by carbonitriles polymerization reaction under the ionothermal condition, and the functionalized CTFs were achieved through the rational design of monomer to improve the gas capture and separation performance. In this paper, a class of porous benzodiimidazole-containing covalent triazine frameworks (**CTF-DIs**) was successfully prepared via ionothermal trimerizations from benzo[1,2-*d*:4,5-*d*']diimidazole based dicyano monomer (**BCBDI**). The N_2 adsorption isotherms at 77 K reveal high BET surface areas of **CTF-DIs** up to 1877 $m^2 g^{-1}$. The effects of reaction temperature and the ratio of monomer to $ZnCl_2$ on the pore characteristics of the **CTF-DIs** were investigated. The highest uptake value for CO_2 is 89.2 $cm^3 g^{-1}$ for **CTF-DI-7** at 273 K and 1 bar. Excitingly, **CTF-DI-6** demonstrates the highest CO_2/N_2 selectivity of 53 and the significant CO_2/CH_4 selectivity of 15 at 273 K and 1 bar, according to IAST, due to the existence of abundant active nitrogen species. These results clearly demonstrate the **CTF-DIs** are likely to be promising candidates for CO_2 capture and separation field.

1. Introduction

As the economic development of the past few decades, the matter of global warming and ocean acidification has been an undesirable trend. The prime cause of this phenomenon is the rapid increase in atmospheric carbon dioxide levels caused by the burning of fossil fuels [1]. To solve this problem, the development of efficient, low-cost, recyclable carbon dioxide capture and storage (CCS) technology is of great importance. Compared with amine scrubbing (amine washing) and chilled ammonia technologies for CO_2 separations [2,3], porous materials as solid-state adsorbents are considered to be the most promising technology for this application due to their low-equipment cost, environmental friendliness, and easy regeneration [4], such as activated carbons [5], porous silica [6], zeolites [7], metal-organic frameworks (MOFs) [8–10], porous organic polymers (POPs) [11] and so on. Different from MOFs linking by coordination bonds, POPs show high physical and chemical stability and low skeletal density because they are linked by covalent bonds by homopolymerization or heteropolymerization of organic building blocks containing light elements (C, H, N, O, B, Si, etc.). They have other advantages over other conventional porous materials, such as rational design flexibility, high specific surface area and ease of modification, endowing them diverse potential applications in sensing [12], catalysis [13], gas capture and separations [14], energy fields [15], and proton conduction [16].

POPs include a variety of materials such as porous aromatic frameworks (PAFs) [17], polymers of intrinsic microporosity (PIMs) [18], hyper-cross-linked polymers (HCPs) [19], covalent organic frameworks (COFs) [20], conjugated microporous polymers (CMPs) [21], covalent triazine frameworks (CTFs) [22,23], and so on. CTFs are generally prepared by carbonitriles polymerization reaction under the ionothermal condition [22], which only requires cheap catalysts like $ZnCl_2$, and does without organic solvent. So, compared with noble-metal-catalyzed synthetic reactions [24,25], the synthetic process of CTFs can significantly reduce economic costs and pollution. For CTFs, apart from their high BET surface area and thermal stability, the high nitrogen content of CTFs endows them with the strong affinity between the frameworks and gas molecules. Lately, CTFs have been demonstrated to be superior to other porous materials in CO_2 capture or selective adsorption, and tremendous efforts have been devoted to further improve the CO_2 capture capacity by the usage of CO_2-philic groups,

* Corresponding author.
** Corresponding author. State Key Lab of Inorganic Synthesis and Preparative Chemistry, Jilin University, Changchun, 130012, PR China.
E-mail addresses: xiaoweisong@jlu.edu.cn (X. Song), liangzq@jlu.edu.cn (Z. Liang).

https://doi.org/10.1016/j.micromeso.2018.10.001
Received 31 July 2018; Received in revised form 30 September 2018; Accepted 1 October 2018
Available online 02 October 2018
1387-1811/

including Tröger's base [26], fluorine rich moieties [27], N-heterocyclic [28,29], fluorene groups [30], porphyrins [31], etc. Meanwhile, previous research confirmed by El-Kaderi and co-workers that benzodiimidazole groups would reinforce the binding affinity between the frameworks and CO_2, and a series of benzimidazole-linked polymers (BILPs) has been synthesized [32,33]. They developed the synthesis of triazine-based benzodiimidazole-linked polymer (TBILP-1), but it shows low BET surface area ($330\ m^2\ g^{-1}$) and CO_2 uptakes ($2.65\ mmol\ g^{-1}$ at 273 K and 1 bar) [34]. On the other hand, most of BILPs were synthesized via solution polycondensation reactions between aryl-aldehydes and aryl-*o*-diamine (easily oxidized), and the reaction conditions must be controlled strictly, including temperatures as low as −30 °C and strict anhydrous conditions, etc. In another study, Han et al. reported a new alternative approach to prepare polybenzimidazoles by Suzuki coupling polymerization between halo-benzodiimidazole and aromatic boronic acids, but the obtained PPBI-2 also exhibits low BET surface area ($158\ m^2\ g^{-1}$) and CO_2 uptake ($1.39\ mmol\ g^{-1}$ at 273 K and 1 bar) [35]. Subsequently, Wang and co-workers reported the CTF-BIs containing benzimidazole groups synthesized by the trimerization of dicyano benzimidazole under ionothermal conditions [36]. Increasing the length of the building units can afford materials with large pore volumes and high BET surface areas, and incorporation of benzodiimidazole moieties will enhance the affinity of CO_2 between CTFs.

With these considerations in mind, herein, we propose an effective synthetic strategy for benzodiimidazole-containing covalent triazine frameworks (**CTF-DIs**). First, we design and synthesize a novel benzo[1,2-*d*:4,5-*d*']diimidazole derived dicyano monomer, 2,6-bis(4-cyanophenyl)-1,5-dihydro-benzo[1,2-*d*:4,5-*d*']diimidazole (**BCBDI**), by aldimine condensation reaction. Then, **CTF-DIs** were prepared by ionothermal polymerization of **BCBDI** in $ZnCl_2$. A series of experiments were designed to investigate the effects of temperature and the ratio of monomer to $ZnCl_2$ on the pore characteristics of the **CTF-DIs**. Finally, we carefully explored the CO_2 capture and the selective adsorption of CO_2 over N_2 and CH_4. The highest uptake values for CO_2 ($89.2\ cm^3\ g^{-1}$) were observed for **CTF-DI-7** at 273 K and 1 bar. Excitingly, **CTF-DI-6** demonstrates the highest CO_2/N_2 selectivity of 53 and the significant CO_2/CH_4 selectivity of 15 at 273 K and 1 bar, according to the ideal adsorbed solution theory (IAST). All these results clearly indicate the proposed ionothermal reaction of benzodiimidazole dicyano monomer is an effective method to synthesize benzodiimidazole-containing covalent triazine frameworks for CO_2 capture and gas separation.

2. Experimental section

2.1. Materials

Except for the **BCBDI** monomer, all other chemicals and solvents were obtained from commercial sources and used as received without further purification. Zinc chloride (Sinopharm Chemical Reagent Co.,Ltd, anhydrous, 98%) was dried for 12 h under vacuum at 180 °C before use. Benzene-1,2,4,5-tetraamine tetrahydrochloride (Zhengzhou Alfa, 95%), 4-cyanobenzaldehyde (Innochem, 98%) and $NaHSO_3$ (Tianjing Guangfu Technoligy Development Co., Ltd, 99%) were used to synthesis the **BCBDI** monomer. All solvents were purchased at Beijing Chemical Works.

2.2. Characterizations

Fourier transform infrared spectra (FTIR) were recorded in the range of 400–4000 cm^{-1} on a Bruker IFS-66-V/S FT-IR spectrometer with KBr pellets. The solid-state ^{13}C cross-polarization/magic-angle spinning (CP/MAS) nuclear magnetic resonance (NMR) spectra were measured on a Bruker AVANCE III 400 MHz NMR spectrometer. ^1H and ^{13}C NMR spectra were recorded at room temperature using a Varian Mercury spectrometer operating at frequencies of 300 and 75 MHz, respectively. Powder X-ray diffraction (PXRD) patterns were obtained on a Rigaku D-Max 2550 diffractometer using Cu-Ka radiation (λ = 1.5418 Å) in a 2θ range of 4–70° with a scan speed of 6° min^{-1} at room temperature. Thermogravimetric analyses (TGA) were performed on a PerkinElmer TGA-7 thermogravimetric analyzer in an air atmosphere/nitrogen atmosphere at a heating rate of 10 °C min^{-1} from room temperature to 800 °C. Scanning electron microscopy (SEM) images were taken on a JSM-6700 M scanning electron microscope operating at 10 kV. Transmission electron microscopy (TEM) images were recorded on a TECNAI F20 with an acceleration voltage of 200 kV. Gas (N_2, CO_2, CH_4) sorption properties and surface areas of samples were measured using a Micromeritics ASAP 2020 surface area and porosity analyzer. The pore size distributions (PSDs) are presented by using the adsorption branch of the isotherms by the nonlocal density functional theory (NLDFT) slit-pore model. The experiment of CO_2 cyclic adsorption and regeneration of **CTF-DI-7** were performed on a PerkinElmer TGA-7 thermogravimetric analyzer. The conditions of test were 25–80 °C at ambient pressure. Water adsorption isotherms were measured on a Hiden IGAsorp machine at 298 K. All samples were degassed at 120 °C for 12 h under vacuum before analyses.

2.3. Synthesis of 2,6-bis(4-cyanophenyl)-1,5-dihydro-benzo[1,2-d:4,5-d'] diimidazole (BCBDI)

In a 250 mL three necked round bottom flask, benzene-1,2,4,5-tetraamine tetrahydrochloride (1.704 g, 6 mmol), 4-cyanobenzaldehyde (1.965 g, 15 mmol) and $NaHSO_3$ (1.872 g, 18 mmol) were dissolved in N,N-dimethylacetamide (100 mL) and the mixture was stirred at 140 °C for 24 h. Then the reaction mixture was poured into water (300 mL) after cooling. Filtration and recrystallization in ethyl acetate afforded **BCBDI** as a dark yellow solid (1.765 g, 4.90 mmol, 81.7% yield). ^1H NMR (300 MHz, DMSO-d_6, δ, ppm): 8.35 (d, J = 8.6 Hz, 4H), 8.06 (d, J = 8.6 Hz, 4H), 7.83 (s, 2H). HRMS (ESI) calcd. for $C_{22}H_{13}N_6^+$ ($[M + H]^+$): 361.1196, found: 361.1201.

2.4. Synthesis of the CTF-DIs

BCBDI (360 mg, 1 mmol) and anhydrous $ZnCl_2$ (2, 5, 8, 10 and 20 eq.) were transferred into an ampoule under inert N_2 atmosphere (Scheme 1). The ampoule was evacuated by vacuum pump, sealed and heated at the rate of 1 °C min^{-1} to 550 °C and maintained at this temperature for 40 h. After cooling to room temperature, the ampoule was opened cautiously. Furthermore, the crude product was carefully ground and then agitated thoroughly under HCl solution (2 M) for 24 h to remove most of the $ZnCl_2$. Finally, the material was rinsed thoroughly using deionized water and ethanol, extracted by Soxhlet with water and THF, dried in a vacuum at 120 °C, weighed and calculated final yield. We find the addition of 8 eq. $ZnCl_2$ led to higher BET surface areas, so other **CTF-DIs** were synthesized under 400, 450, 500 and 600 °C using a similar procedure and the same addition of $ZnCl_2$ (8 eq.) to investigate the effect of reaction temperature (Table 1).

3. Results and discussion

3.1. Synthesis and characterization of the CTF-DIs

To embed the benzodiimidazole building unit into the CTFs, the benzodiimidazole dicyano monomer **BCBDI** was synthesized with a good yield by the oxidative coupling reaction of benzene-1,2,4,5-tetraamine tetrahydrochloride and 4-cyanobenzaldehyde in DMA at 140 °C (Scheme 1). The chemical structures of **BCBDI** was approved by ^1H NMR (Fig. S1) and HRMS (Fig. S2). **BCBDI** shows relative good thermal stability according to the TGA curve (Fig. S3). The synthetic procedure of the **CTF-DIs** is constructed by the ionothermal trimerization reaction of **BCBDI** monomer using $ZnCl_2$ as both catalyst and solvent [22]. As reported previously, the porosity properties of CTFs are

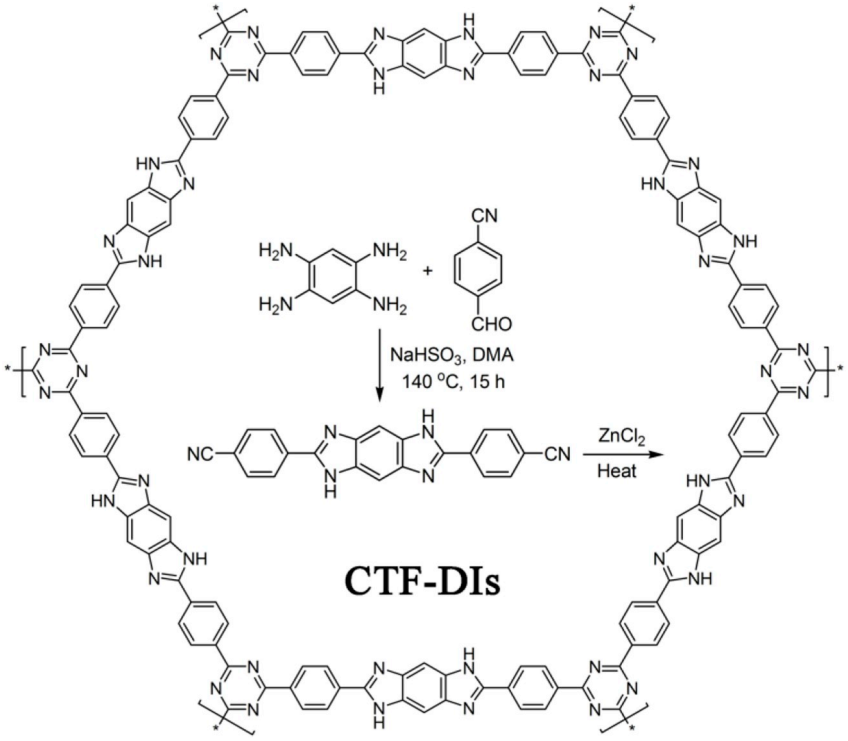

Scheme. 1. Synthetic schematic representation of **CTF-DIs**.

greatly affected by the reaction temperature and molar ratios of monomer to $ZnCl_2$ [36]. Thus, several synthetic conditions at different temperatures and molar ratio (Table 1) were used to explore the porous properties of **CTF-DIs**. First, **CTF-DI-1–5** were synthesized at 550 °C with the molar ratio of **BCBDI**/$ZnCl_2$ at 1:2, 1:5, 1:8, 1:10 and 1:20, respectively. Then, the trimerization of **BCBDI** at 400, 450, 500 and 600 °C yielded **CTF-DI-6–9** under the molar ratio of **BCBDI**/$ZnCl_2$ at 1:8. All of the above reaction times are 40 h. In all cases, the black products were carefully ground into fine powder, and then washed thoroughly with HCl aqueous solution (2 M), water and ethanol. Finally, the **CTF-DIs** were extracted by Soxhlet using water and THF, respectively. The final yields are in the range of 75–91%.

The formation of triazine unit can be verified by FT-IR analysis, and the IR spectra of the monomer **BCBDI**, **CTF-DI-6** (400 °C), **CTF-DI-3** (550 °C) and other **CTF-DIs** are shown in Fig. 1a, S4 and S5. After reaction, the characteristic nitrile stretching band at 2231 cm^{-1} almost completely disappears in the **CTF-DIs**, showing that the nitrile groups of **BCBDI** have been completely consumed. In the meantime, the characteristic stretching bands of triazine rings appear at 1370 and 1578 cm^{-1} in all **CTF-DIs**, creating an overlap with nearby peaks, although the bands are weakly and featureless (Figs. S4 and S5). These results indicate the nitrile groups have been converted into triazine rings. As those of previous works reported [30], when the reaction temperatures were gradually increased, the triazine and benzodiimidazole frameworks were partially carbonized. So when the temperature reaches 600 °C, the material is transformed into triazine-based porous carbon.

The solid state ^{13}C CP/MAS NMR spectra was used to indicate the local structures of **CTF-DIs** at the molecular level. The ^{13}C CP/MAS NMR spectra and the assignment of all resonances of **BCBDI**, **CTF-DI-3** and **CTF-DI-6** are displayed in Fig. S6. The ^{13}C NMR spectrum of **BCBDI** exhibits the eight carbon signals at 148.6, 139.2, 132.9, 125.3, 118.2, 112.9, 103.8 and 97.9 ppm. The signals of the nitrile carbons and nearby aromatic carbons at 103.8 and 97.9 ppm are almost disappeared in the ^{13}C NMR spectra of **CTF-DI-3** and **CTF-DI-6**, indicating the high degree of polymerization. This result is consistent with the previously described FT-IR results [28]. The signal located at 148.6 and 139.2 ppm in **BCBDI** should be ascribed to the carbons in imidazole units and aromatic carbons linked imidazole [32], which are existed obviously in **CTF-DI-6**, indicating the benzodiimidazole moieties are maintained.

Table 1
A summary of the reaction conditions and pore characteristics for the **CTF-DIs** based on N_2 isotherms collected at 77 K.

Samples	Molar ratio of BCBDI/$ZnCl_2$	Reaction conditions	Yield (%)	S_{BET} [a] [$m^2\ g^{-1}$]	S_{Lang} [b] [$m^2\ g^{-1}$]	$V_{0.1}$ [c] [$cm^3\ g^{-1}$]	V_{tot} [d] [$cm^3\ g^{-1}$]	$V_{0.1}/V_{tot}$
CTF-DI-1	1:2	550 °C	90	26	37	0.0097	0.021	0.47
CTF-DI-2	1:5	550 °C	91	420	579	0.17	0.35	0.48
CTF-DI-3	1:8	550 °C	89	1877	2611	0.65	1.41	0.46
CTF-DI-4	1:10	550 °C	90	1769	2433	0.61	2.54	0.24
CTF-DI-5	1:20	550 °C	86	1207	1699	0.44	0.84	0.52
CTF-DI-6	1:8	400 °C	89	697	947	0.29	0.99	0.30
CTF-DI-7	1:8	450 °C	80	1300	1780	0.54	1.67	0.32
CTF-DI-8	1:8	500 °C	75	1749	2452	0.66	2.27	0.29
CTF-DI-9	1:8	600 °C	77	1228	1758	0.43	1.04	0.42

[a] BET surface areas calculated over the pressure range 0.05–0.20 P/P_o at 77 K.
[b] Langmuir surface area calculated from the N_2 adsorption isotherm by application of the Langmuir equation.
[c] $V_{0.1}$, pore volume at $P/P_o = 0.1$. [d] V_{tot}, total pore volume calculated at $P/P_o = 0.99$.

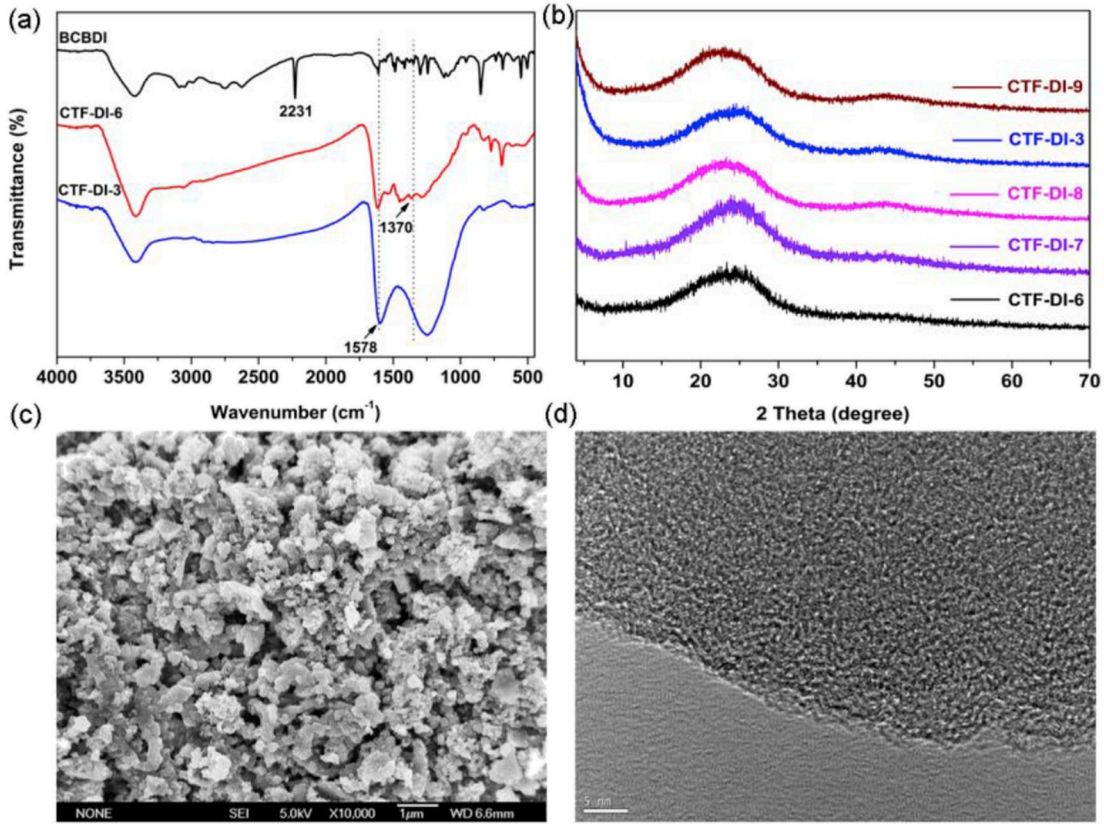

Fig. 1. (a) FT-IR spectra of monomer **BCBDI** and **CTF-DI-3** and **CTF-DI-6**. (b) PXRD patterns of **CTF-DI-3**, **CTF-DI-6**, **CTF-DI-7**, **CTF-DI-8** and **CTF-DI-9**. (c) FE-SEM image of **CTF-DI-3**. (d) TEM image of **CTF-DI-3**.

While in **CTF-DI-3**, the intensity is relatively weak. The characteristic signals of the triazine unit at around 170 ppm are so weak that it could not be found, due to the high temperature leading to the partial graphitization of materials, which has been reported previously [37,38].

By powder X-ray diffraction (PXRD), the crystallinity of the **CTF-DIs** are verified in Fig. 1b and S7. As expected, the typical peak at around 24.7° indicates the amorphous nature of the polymers, which is similar to the reported results [22]. The **CTF-DIs** are composed of generally amorphous structures and partially graphitized. Thermal stability of the triazine frameworks was further studied by thermogravimetric analysis (TGA) under air and nitrogen atmosphere, respectively. As shown in Fig. S8, **CTF-DI-3** exhibits high stability up to 450 °C under air atmosphere and high weight reserved at 800 °C under N_2. The weight loss before 100 °C is assigned to the adsorption of gas and water vapor, which is similar to most of the reported POPs. The surface morphologies of samples were observed by FE-SEM. As displayed in Fig. 1c, **CTF-DI-3** are composed of aggregated particles with irregular sizes and shapes. HR-TEM images were clearly displayed that their disordered porous structural nature by the alternating areas of light and dark contrast (Fig. 1d).

3.2. Porous properties of *CTF-DIs*

To characterize the porosity of **CTF-DIs**, nitrogen adsorption/desorption isotherms were recorded at 77 K. All sample were activated under a dynamic vacuum at 120 °C for 12 h. Fig. 2a and c shows that, except for **CTF-DI-1**, all the isotherms exhibit a steep nitrogen uptake in the low-pressure region ($P/P_o < 0.01$), characteristic for microporosity, in the meantime the isotherms also exist hysteresis loops, implying the presence of mesopores and/or macropores. According to the IUPAC classification [39], all eight **CTF-DIs** showed type I N_2 sorption isotherms with type IV characters at higher relative pressure with Brunauer-Emmett-Teller (BET) surface areas varying from 420 to 1877 $m^2 g^{-1}$ (Table 1). As previously reported CTFs [22,23], **CTF-DIs** also show the same phenomenon that the amount of $ZnCl_2$ and the reaction temperature have huge impact on the pore characteristics of the obtained materials. To optimize the reaction conditions for polymerization, a series of conditions were set up to study the above two cases. First, five different **BCBDI**/$ZnCl_2$ ratios (1:2, 1:5, 1:8, 1:10 and 1:20) were investigated at 550 °C. Because that $ZnCl_2$ is both catalyst and solvent in the trimerization reaction, the amount of $ZnCl_2$ has a significant effect on the pore properties. With the increase in the ratio of **BCBDI**/$ZnCl_2$ from 1:2 to 1:20, the BET surface area of the polymeric frameworks gradually increases and then decreases. The BET surface area of **CTF-DI-3** obtained at 1:8 is the largest, and the value is 1877 $m^2 g^{-1}$. The BET surface area of **CTF-DI-3** is much higher than that of CTF-BIs synthesized from 2-(4-cyanophenyl)-1H-benzo[*d*]imidazole-5-carbonitrile (DCBI, 1549 $m^2 g^{-1}$) under similar conditions [36]. The reason is that **BCBDI** has a longer molecular structure than DCBI. In addition, the representative structures of **CTF-DIs** are same to TBILP-1 reported by El-Kaderi, while the BET surface areas of **CTF-DIs** are much higher than that of TBILP-1 (330 $m^2 g^{-1}$) [34]. Compared to other **CTF-DIs**, **CTF-DI-4** prepared using **BCBDI**/$ZnCl_2$ ratio of 1:10 at 550 °C shows the most remarkable of type IV isotherms, indicating there are abundant meso- and macropores in this material. The pore size distributions (PSDs) of **CTF-DI-4** shows a wide range between 1.09 and 31.79 nm (Fig. 2b), while the PSDs of **CTF-DI-3** and **CTF-DI-5** are mainly in the range from 1.00 to 5.00 nm (1.27 nm and 2.5 nm). This is a definite sign that appropriately increasing the amount of $ZnCl_2$ could promote the content of meso- and/or macroporosity for **CTF-DIs**. In addition, the effect of reaction temperature on porous properties of **CTF-DIs** was evaluated using the fixed **BCBDI**/$ZnCl_2$ ratio of 1:8 at 400 (**CTF-DI-6**), 450 (**CTF-DI-7**), 500 (**CTF-DI-8**) and 600 °C (**CTF-DI-9**). As shown in Fig. 2c, the adsorption isotherms of them are similar to that of

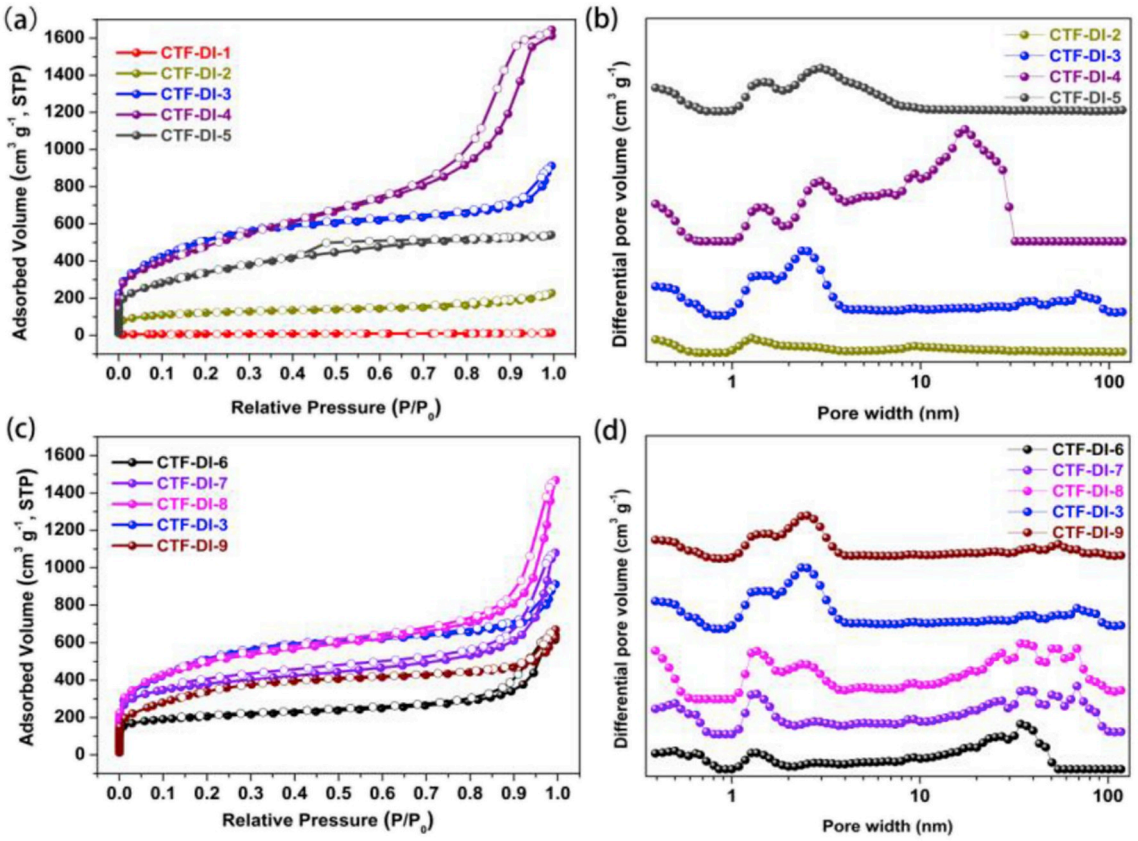

Fig. 2. Pore characteristics of **CTF-DIs**. (a, c) N_2 adsorption and desorption isotherms at 77 K for **CTF-DIs** (filled symbols for adsorption and unfilled symbols for desorption); (b, d) pore size distributions (PSDs) of **CTF-DI-2–9** calculated by the NLDFT method.

CTF-DI-3, and the BET surface areas of **CTF-DI-6–9** are 697, 1300, 1749 and 1228 $m^2 g^{-1}$, respectively. When the relative pressure reached 0.8, the nitrogen adsorption capacity of **CTF-DIs** increased significantly, which was attributed to macroporous or stacking pores in the samples (Fig. 2d). The PSDs of **CTF-DI-6** and **CTF-DI-7** is mainly divided into two parts. The first is the micropore region dominated by widely distributed ultramicropores (< 0.7 nm) and 1.27 nm, and the second is the mesopores and/or macropores region (> 10 nm), because of the larger molecular size of **BCBDI**. The total pore volumes of **CTF-DI-2–9** calculated at $P/P_o = 0.99$ are up to 2.54 $cm^3 g^{-1}$, and the micropore volumes ($P/P_o = 0.01$) are in the range of 0.17–0.66 $cm^3 g^{-1}$ (Table 1).

3.3. Gas uptake studies

Owing to their high surface areas and CO_2-philic groups of benzodiimidazole and triazine, we explored the CO_2 capture properties of **CTF-DIs**. As shown in Fig. 3, Fig. S9, and Table 2, the CO_2 adsorption/desorption isotherms of **CTF-DIs** were measured at 273 and 298 K, respectively. All CO_2 adsorption and desorption isotherms are completely reversible. For **CTF-DI-2–5** synthesized at 550 °C with different molar ratios of monomer to $ZnCl_2$, the CO_2 uptakes at 273 K and 1 bar are 33.5 $cm^3 g^{-1}$ for **CTF-DI-2**, 80.4 $cm^3 g^{-1}$ for **CTF-DI-3**, 67.6 $cm^3 g^{-1}$ for **CTF-DI-4** and 50.9 $cm^3 g^{-1}$ for **CTF-DI-5**, respectively. The CO_2 adsorption amounts are in the following trend: **CTF-DI-3** > **CTF-DI-4** > **CTF-DI-5** > **CTF-DI-2**, which shows the similar tendency with their BET surface areas. For **CTF-DI-3** and **CTF-DI-6–9** prepared at different temperature with the same amount of $ZnCl_2$, the CO_2 uptakes ranged from 59.7 to 89.2 $cm^3 g^{-1}$ at 273 K and 1 bar. **CTF-DI-7** displays the highest CO_2 uptake (89.2 $cm^3 g^{-1}$), although the BET surface area is less than that of **CTF-DI-3**, **CTF-DI-4** and **CTF-DI-8**. The CO_2 uptake of **CTF-DI-7** (3.98 mmol g^{-1}/89.2 $cm^3 g^{-1}$) is much higher than TBILP-1 (2.65 mmol g^{-1}/59.4 $cm^3 g^{-1}$) [34] at 273 K and 1 bar, but slightly lower than CTF-BIs (2.51–4.91 mmol g^{-1}/56.3–110.5 $cm^3 g^{-1}$) at 273 K and 1.1 bar [36]. While the CO_2 uptakes of **CTF-DI-3** and **CTF-DI-7** are higher than other previously reported CTFs, such as CTF-1 (55.3 $cm^3 g^{-1}$) [40], CTF-1-600 (85.6 $cm^3 g^{-1}$) [40], PHCTF-1-7 (42.8–52.4 $cm^3 g^{-1}$) [41], PCTF-1–7 (41.5–73 $cm^3 g^{-1}$) [42,43] and CTF-FUM-350 (78.2 $cm^3 g^{-1}$) [44] at 273 K and 1 bar. The reason is that the positive impact of benzodiimidazole building units in the framework will increase the CO_2-philicity of **CTF-DIs**. However, **CTF-DIs** show lower adsorption abilities than the recently reported FCTF-1 (104.6 $cm^3 g^{-1}$) [40] and HAT-CTF (141.12 $cm^3 g^{-1}$) [45] at the same conditions. Even compared with those reported for porous organic frameworks PAF-1 (46.3 $cm^3 g^{-1}$) [46], TPI-1 (54.5 $cm^3 g^{-1}$) [47],functionalized CMPs (35.8–40.3 $cm^3 g^{-1}$) [48], and porous carbon monolith HCM-DAH-1 (73.9 $cm^3 g^{-1}$) [49]. **CTF-DI-3** and **CTF-DI-7** also showed a greater advantage for the CO_2 uptake capacities. It is interesting that they are even superior to commercially available BPL carbon (46.8 $cm^3 g^{-1}$, at 1 bar and 273 K) [50].

It is worth noting that the BET surface of **CTF-DI-3** is much higher than that of **CTF-DI-7** (1877 $m^2 g^{-1}$ vs. 1300 $m^2 g^{-1}$), but has a lower CO_2 uptake capacity (80.4 $cm^3 g^{-1}$ vs. 89.2 $cm^3 g^{-1}$). This can be attributed to two reasons. First, **CTF-DI-7** has a rich ultramicroporous region compared to **CTF-DI-3**. It is generally believed that the ultramicroporous region is favorable for the adsorption of CO_2 due to the narrowness pores enhance the interaction of CO_2 with multiple framework surfaces [42]. Second, the partial pyrolysis of benzimidazole units at high temperatures is resulted in a decrease in nitrogen content as the recently reported [36]. This indicates that the CO_2 adsorption capacity is not matching to the BET surface area. Hence, simply increasing the BET surface area could not increase the CO_2 capture ability.

Under realistic conditions, the flue gas usually contains the low CO_2 concentration (approximately 15% CO_2 at a total pressure of 1 bar), the

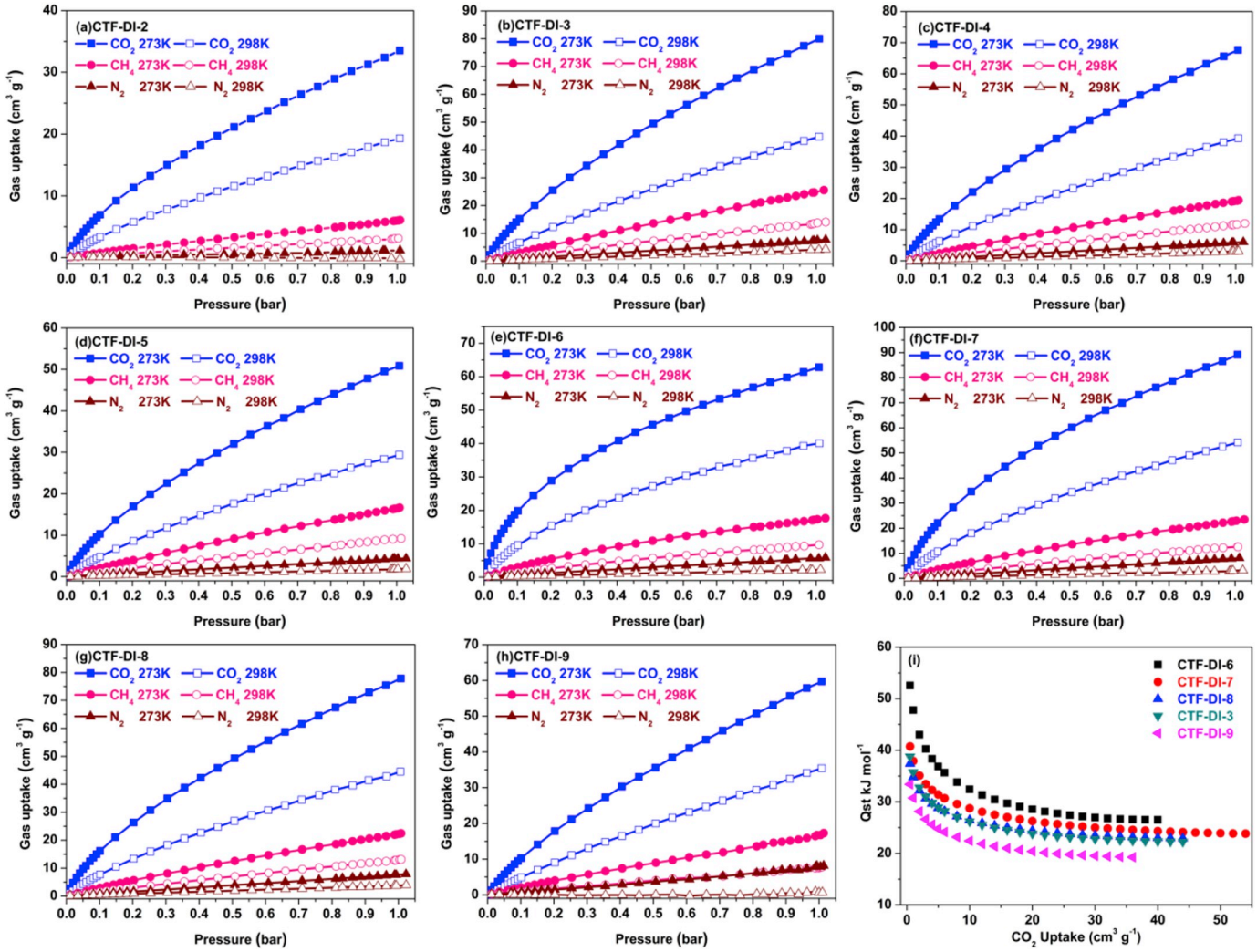

Fig. 3. (a–h) Adsorption isotherms of CO_2, N_2, and CH_4 in all **CTF-DIs** at 298 and 273 K; (I) the calculated isosteric heat values of CO_2 adsorption of **CTF-DI-3** and **CTF-DI-6–9**.

Table 2
CO_2 uptakes and CO_2 selectivities over N_2 and CH_4 at 273 K of **CTF-DI-2 − 9**.

Samples	SA_{BET} [m^2 g^{-1}]	CO_2 uptake (cm^3 g^{-1})[a]		Q_{st} for CO_2 (kJ/mol)	CO_2 selectivity calculated from initial slope[b]		CO_2 selectivity calculated using IAST[c]	
		273 K	298 K		CO_2/CH_4	CO_2/N_2	CO_2/CH_4	CO_2/N_2
CTF-DI-2	420	33.5	19.3	32.4	15	70	14(12)	35
CTF-DI-3	1877	80.4	44.7	38.7	8	29	6(5)	26
CTF-DI-4	1769	67.6	39.3	40.1	9	34	8(7)	42
CTF-DI-5	1207	50.9	29.4	37.2	8	37	6(5)	27
CTF-DI-6	697	62.8	40.0	52.6	20	73	15(12)	53
CTF-DI-7	1300	89.2	54.2	40.7	13	47	11(9)	41
CTF-DI-8	1749	77.8	44.5	37.4	10	34	8(6)	35
CTF-DI-9	1228	59.7	35.4	33.4	6	17	6(6)	14

[a] CO_2 uptake at 1 bar.
[b] Selectivities of CO_2/N_2 and CO_2/CH_4 calculated from initial slope.
[c] CO_2/N_2 and CO_2/CH_4 selectivities calculated based on the IAST method from a gas mixture ratio of 0.15/0.85 and 0.05/0.95 (0.5/0.5) at 1 bar, respectively.

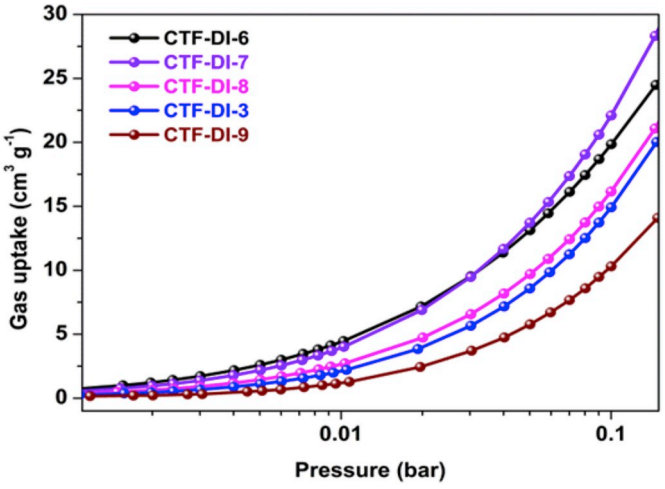

Fig. 4. Adsorption isotherms of CO_2 in all **CTF-DIs** at 273 K and 0.15 bar, shown in logarithmic abscissae.

porous sorbents should have the ability to adsorb large amounts of CO_2 at ~0.15 bar. **CTF-DI-7** exhibits the best uptake performance (28.3 cm^3 g^{-1}) at 273 K and 0.15 bar among **CTF-DIs** (Table S1), which is significantly higher than recently reported CTF-CSUs (15.3–29.0 cm^3 g^{-1}) [51]. In fact, in the low-pressure regime, the strong electrostatic interactions between the surface functional groups (the imidazole N—H) of **CTF-DIs** and CO_2 molecules play a significant part of the CO_2 adsorption behavior. So **CTF-DI-6** and **CTF-DI-7**

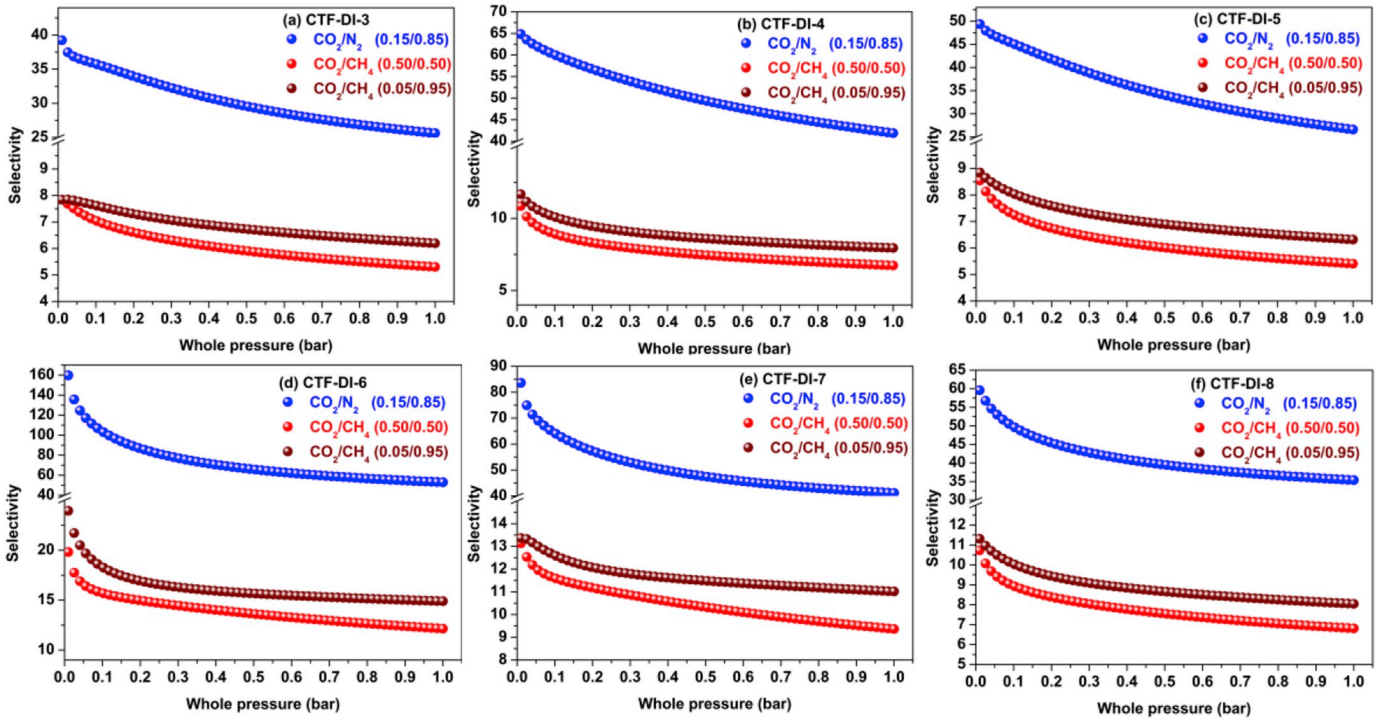

Fig. 5. (a–f) IAST selectivities for the 0.15/0.85 CO_2/N_2 mixture (blue squares), the 0.50/0.50 CO_2/CH_4 mixture (red circles), and the 0.05/0.95 CO_2/CH_4 mixture (wine triangles) for **CTF-DI-3–8**. (For interpretation of the references to colour in this figure legend, the reader is referred to the Web version of this article.)

synthesized at the lower temperature retain more complete functional groups, the interaction with the CO_2 molecules is stronger and the CO_2 adsorption capacity is better at low pressure (Fig. 4). **CTF-DIs** also exhibit the excellent CO_2 adsorption capacity at 273 K and 0.50 bar (crude biogas), up to 60.2 $cm^3\ g^{-1}$ for **CTF-DI-7** (Table S1). The excellent CO_2 uptake at both low and moderate pressure suggests the actual suitability of benzodiimidazole-containing covalent triazine frameworks (**CTF-DIs**) for CO_2 capture from flue gas or crude biogas under more realistic conditions.

To investigate the affinity between CO_2 and the framework of **CTF-DIs**, the isosteric CO_2 adsorption enthalpies (Q_{st}) are calculated using the Clausius–Clapeyron equation (Fig. 3I and S10). For **CTF-DI-2–5** synthesized at 550 °C with different molar ratios of monomer to $ZnCl_2$, the Q_{st} values are 32.4 kJ mol^{-1} for **CTF-DI-2**, 38.7 kJ mol^{-1} for **CTF-DI-3**, 40.1 kJ mol^{-1} for **CTF-DI-4** and 37.2 kJ mol^{-1} for **CTF-DI-5**, respectively. The Q_{st} values are in the following trend: **CTF-DI-4** > **CTF-DI-3** > **CTF-DI-5** > **CTF-DI-2**, which shows the nearly same tendency with their CO_2 adsorption amounts. For **CTF-DI-3** and **CTF-DI-6–9** prepared at different temperature with the same amount of $ZnCl_2$ as catalysts, the Q_{st} values ranged from 33.4 kJ mol^{-1} to 52.6 kJ mol^{-1}. As the reaction temperature was increased from 400 to 600 °C, the Q_{st} values decreased gradually. This trend is consistent with the results of the elemental analysis (Table S2), in which the loadings of N are in the following trend: **CTF-DI-6** > **CTF-DI-7** > **CTF-DI-8** > **CTF-DI-3** > **CTF-DI-9**. The phenomenon can be attributed again to the partial pyrolysis of the triazine and benzimidazole rings leading to the decrease in the affinity of **CTF-DIs** with CO_2, as mentioned above. With the increase CO_2 adsorption amounts, the Q_{st} values decrease rapidly from the initial high enthalpies of adsorption. They are mainly attributed to that the CO_2 molecule has stronger electrostatic interactions toward the nitrogen-rich polar binding sites, both from benzodiimidazole and triazine rings, than CO_2 itself. Meanwhile, The Q_{st} values of all these **CTF-DIs** are near or higher than 30 kJ mol^{-1}, and even up to 50 kJ mol^{-1} at low coverage, among those **CTF-DI-6** displays the highest Q_{st} value up to 50 kJ mol^{-1}. The Q_{st} values of **CTF-DIs** are within the scope of 32.4 kJ mol^{-1} and 52.6 kJ mol^{-1}, which are higher than those of many other POPs, for example CMP (27–33 kJ mol − 1) [48], HCP-1 (24 kJ mol − 1) [52], and NOPs (28–37 kJ mol − 1) [53]. Overall, the Q_{st} values of all the **CTF-DIs** not exceeding 60 kJ mol^{-1} demonstrate that they are considered be useful for the efficient reversible adsorption and desorption of CO_2 in CCS operations.

To assess the ability of the CO_2 adsorption/desorption cycles, we conducted multiple CO_2 adsorption cycle tests for the most adsorbed **CTF-DI-7** under ambient pressure from 25 to 80 °C. As shown in Fig. S11, **CTF-DI-7** shows a stable CO_2 adsorption capacity and only a small weight change even after more than 10 cycles.

3.4. Ideal selectivities of CO_2/N_2 and CO_2/CH_4 gas pairs

To further evaluate the potential application of **CTF-DIs** frameworks in selective CO_2 capture over CH_4 and N_2, the single-component

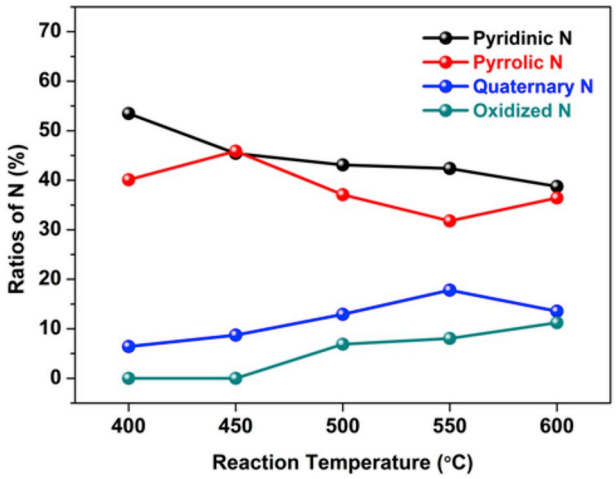

Fig. 6. The ratios of four N-configurations in **CTF-DIs** obtained from different reaction temperatures.

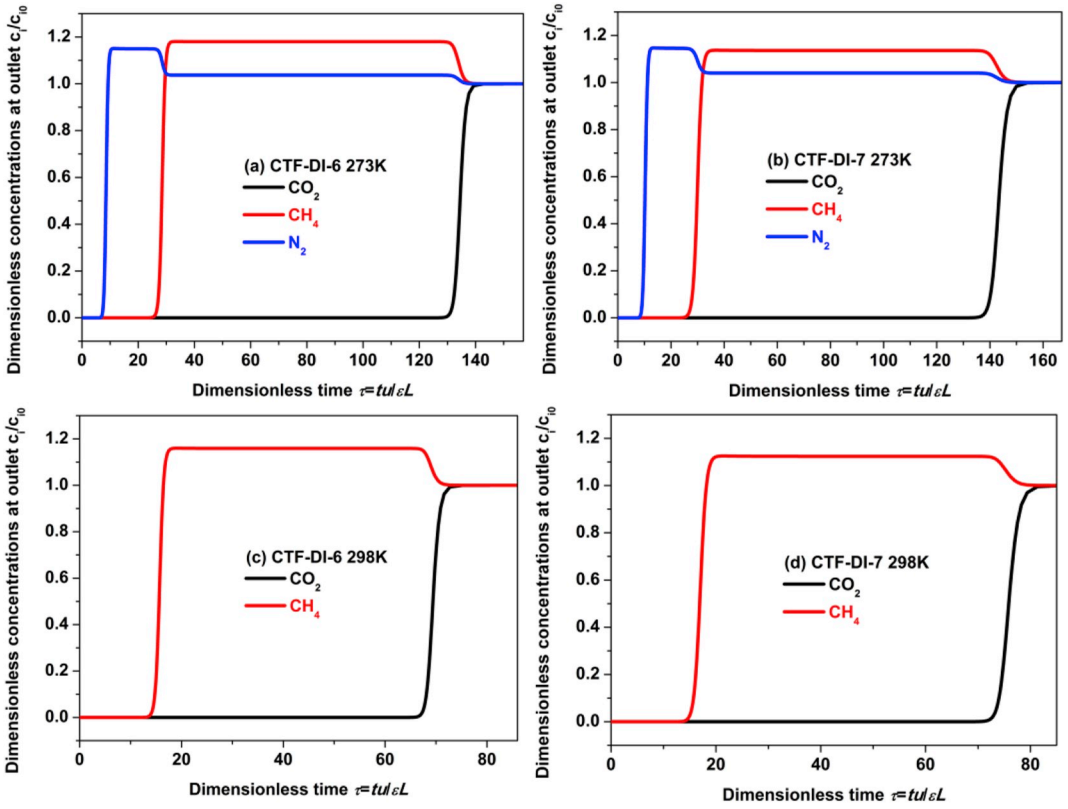

Fig. 7. Transient breakthrough simulation data for equimolar $CO_2/CH_4/N_2$ mixtures operating at a total pressure of 100 kPa and 273 K of **CTF-DI-6** (a) and **CTF-DI-7** (b), and equimolar CO_2/CH_4 mixtures operating at a total pressure of 100 kPa and 298 K of **CTF-DI-6** (c) and **CTF-DI-7** (d).

adsorption isotherms of CH_4 and N_2 at 273 and 298 K were measured, respectively. As shown in Fig. 3, all **CTF-DIs** show much stronger abilities to capture CO_2 than N_2 and CH_4. Therefore, the selectivities for **CTF-DIs** were evaluated using one of the most common methods using the ratio of the initial slopes in the Henry region of the adsorption isotherms. The initial slopes of adsorption isotherms were obtained by a linear fit as shown in Figs. S12–S13. The calculated selectivities was listed in Table 2. The calculated CO_2/N_2 selectivities of **CTF-DIs** were in range of 17–70 at 273 K. The selectivities were comparable with those of triazine-based PCTFs (9–22 at 273 K) [42,43], Cz-POFs (19–37 at 273 K) [54], APOPs (23.8–43.4 at 273 K) [55], LMOP-15 (61.7 at 273 K) [56]. At the same time, the performance of the CO_2/CH_4 selectivities is in range of 6–20 at 273 K (Table 2). The selectivities exceeded previously reported APOPs (5.3–6.7 at 273 K) [55], MPIs (8–12 at 273 K) [57], PPF-1–4 (8.6–11.0 at 273 K) [58].

In order to simulate the practical applications of selective adsorption for CO_2 over N_2 and CH_4, the CO_2/N_2 (0.15:0.85, flue gas) and CO_2/CH_4 (0.5:0.5, landfill gas, and 0.05:0.95, natural gas) adsorption selectivities were calculated by ideal adsorption solution theory (IAST) using the single component adsorption isotherms [59]. As illustrated in Figs. S14 and S15, all of results were obtained through the dual site Langmuir Freundlich (DSLF) model at 273 K and 1 bar and fitted well with the experimental single-component isotherms. As shown in Fig. 5 and S16, the ideal selectivities of CO_2 over N_2 for **CTF-DIs** versus the pressure (0–1 bar) of the mixed gases were in the range of 14–53. The ideal selectivity of CO_2/N_2 calculated from IAST method was basically similar to the results above from initial slope selectivity calculations. Under different reaction temperatures, the CO_2 capacities of **CTF-DI-6** are not superior to other high temperature synthetic **CTF-DIs**, yet the performance of the CO_2/N_2 selectivities improved up to 53 for **CTF-DI-6**. This problem can be explained by X-ray photoelectron spectroscopy (XPS) study, the N 1s core level spectra of **BCBDI** and all **CTF-DIs** obtained from different reaction temperatures are presented in Fig. S17. As expected from its molecular structure, **BCBDI** exhibits two peaks at 398.30 and 397.97 eV which is nonprotonated pyridinic and protonated pyrrolic nitrogen atoms of the imidazole ring, respectively. The frameworks of **CTF-DIs** possessed three or four different nitrogen environments, including pyridinic N (398.34–398.52 eV), pyrrolic N (400.13–400.30 eV), quaternary N (401.28–402.30 eV), and oxidized N (402.32–402.51 eV). For **CTF-DI-6** (400 °C) and **CTF-DI-7** (450 °C), there are three different nitrogen environments. While the polymerization temperature was raised to 500, 550 and 600 °C, the resulting **CTF-DI-8**, **CTF-DI-3** and **CTF-DI-9** possess four different nitrogen environments. With the reaction temperature increases, the decomposition of the triazine and benzodiimidazole frameworks caused the pyridinic N (non-protonated pyridine and in the triazine rings) to gradually decrease, and the contents of quaternary N and oxidized N increase obviously (Fig. 6). In general, the interactions between CO_2 and pyridinic N and pyrrolic N were much stronger than those of quaternary N and N-oxide [32]. These results are consistent with the high Q_{st} of **CTF-DI-6** and **CTF-DI-7**. So the performance of the CO_2/N_2 selectivities is reduced with the reaction temperature increases. The selectivity of **CTF-DIs** was higher than some reported POPs, for example PHCTF-7 (47 at 273 K) [41], CTF-FL (48 at 273 K) [60], CTF-TPC (30 at 273 K) [60], MPI-BPA (24.7 at 273 K) [61], API-6FA (40.8 at 273 K) [61], ALPs (34–44 at 273 K) [62]. At the same time, in Table 2, the ideal selectivity of CO_2/CH_4 calculated from IAST method also retained the same conclusion. The performance of the CO_2/CH_4 (0.05:0.95, natural gas) selectivity at 273 K is reaching ~15 at 1 bar, and reduced from 15 of **CTF-DI-6** to 6 of **CTF-DI-9** with the increase of reaction temperature. Meanwhile, the calculated CO_2/CH_4 (0.50:0.50, landfill gas) selectivities of **CTF-DIs** were in a range of 5–12 at 273 K Therefore, it can be concluded that introducing the benzodiimidazole building units in the triazine frameworks is very useful in CTFs for CO_2 capture and selectivity.

To explore the hydrophobicity or hydrophilicity nature of the

obtained **CTF-DIs**, the water vapor sorption isotherm was recorded at 298 K for the promising **CTF-DI-7** (Fig. S18). **CTF-DI-7** shows Type III isotherms. **CTF-DI-7** has a low water molecule adsorption capacity at low pressure, which embodies the hydrophobicity nature of the pores, and the adsorption amount increases sharply with increasing pressure. The total water vapor sorption is reached 0.66 $g\,g^{-1}$ at $p/p_0 = 0.93$. Compared with DCBP-CTF-1 [27], the pore surface hydrophilicity of **CTF-DI-7** is increased due to the introduction of benzodiimidazole groups.

3.5. Transient breakthrough of mixtures in fixed bed adsorbers

Considering the possible use of **CTF-DIs** as solid adsorbents for gas separation in industrial fixed bed adsorbers, we used the transient breakthrough simulations to properly evaluate the working performance of the promising **CTF-DI-6** and **CTF-DI-7**. Transient breakthrough simulations were carried out for equimolar $CO_2/CH_4/N_2$ mixtures operating at a total pressure of 100 kPa and 273 K, and equimolar CO_2/CH_4 mixtures operating at a total pressure of 100 kPa and 298 K, using the methodology in earlier literature reports, as shown in Fig. 7 [63–66]. The breakthrough times sequence is $CO_2 > CH_4 > N_2$ at 273 K and $CO_2 > CH_4$ at 298 K for **CTF-DI-6** and **CTF-DI-7**, and there is a time interval in the breakthroughs, which is decided by the hierarchy of adsorption strengths. On the basis of the transient breakthrough simulations, we note that the separation performance of both **CTF-DI-6** and **CTF-DI-7** in fixed bed adsorbers are very close to each other. IAST calculations show that **CTF-DI-6** has slightly higher selectivity than **CTF-DI-7**. However, the CO_2 uptake capacity of **CTF-DI-7** is slightly higher than that of **CTF-DI-6**. The performance of industrial fixed bed adsorbers is dictated by a combination of adsorption selectivity and uptake capacity. Comprehensive the IAST method and breakthrough simulation verified, **CTF-DI-6** and **CTF-DI-7** are suitable for selective CO_2 capture and separation from $CO_2/CH_4/N_2$ mixtures.

4. Conclusions

In summary, an effective strategy was developed to obtain highly porous benzodiimidazole-containing covalent triazine frameworks (**CTF-DIs**) via ionothermal polymerization from benzodiimidazole dicyano monomer **BCBDI**. Their porous properties can be tuned from mainly microporous to micro/meso/microporous by changing the reaction conditions including the ratio of catalyst and temperature. The N_2 sorption isotherms at 77 K revealed high BET surface areas for **CTF-DIs** up to 1877 $m^2\,g^{-1}$. Meanwhile, they show high CO_2 uptakes up to 89.2 $cm^3\,g^{-1}$ at 273 K and 1 bar, and high adsorption heats up to 52 $kJ\,mol^{-1}$. Excitingly, **CTF-DI-6** demonstrates the high CO_2/N_2 selectivity up to 53 (273 K, 1 bar) and CO_2/CH_4 selectivity up to 15 (273 K, 1 bar) according to IAST, due to the presence of active N species of benzodiimidazole and triazine. This work illustrates a useful strategy of designing and synthesizing porous benzodiimidazole-containing covalent triazine frameworks to obtain efficient CO_2 capture capability. The obtained **CTF-DIs** are promising candidates for application in the gas capture and separation field.

Acknowledgements

We thank the National Natural Science Foundation of China (Grant Nos. 21471064 and 21621001), the National Key Research and Development Program of China (Grant No. 2016YFB0701100), and the 111 project of the Ministry of Education of China (Grant No. B17020).

Appendix A. Supplementary data

Supplementary data to this article can be found online at https://doi.org/10.1016/j.micromeso.2018.10.001.

References

[1] R.S. Haszeldine, Science 325 (2009) 1647–1652 https://doi.org/10.1126/science.1172246.
[2] G.T. Rochelle, Science 325 (2009) 1652–1654 https://doi.org/10.1126/science.1176731.
[3] U. Desideri, A. Paolucci, Energy Convers. Manag. 40 (1999) 1899–1915 https://doi.org/10.1016/S0196-8904(99)00074-6.
[4] D.M. D'Alessandro, B. Smit, J.R. Long, Angew. Chem. Int. Ed. 49 (2010) 6058–6082 https://doi.org/10.1002/anie.201000431.
[5] L. Wang, R.T. Yang, J. Phys. Chem. C 116 (2012) (2012) 1099–1106 https://doi.org/10.1021/jp2100446.
[6] J.C. Hicks, J.H. Drese, D.J. Fauth, M.L. Gray, G. Qi, C.W. Jones, J. Am. Chem. Soc. 130 (2008) 2902–2903 https://doi.org/10.1021/ja077795v.
[7] J. Zhang, P.A. Webley, P. Xiao, Energy Convers. Manag. 49 (2008) 346–356 https://doi.org/10.1016/j.enconman.2007.06.007.
[8] Z. Zhang, Z.Z. Yao, S. Xiang, B. Chen, Energy Environ. Sci. 7 (2014) 2868–2899 https://doi.org/10.1039/c4ee00143e.
[9] W.M. Bloch, R. Babarao, M.R. Hill, C.J. Doonan, C.J. Sumby, J. Am. Chem. Soc. 135 (2013) 10441–10448 https://doi.org/10.1021/ja4032049.
[10] O. Shekhah, Y. Belmabkhout, Z. Chen, V. Guillerm, A. Cairns, K. Adil, M. Eddaoudi, Nat. Commun. 5 (2014) 4228 https://doi.org/10.1038/ncomms5228.
[11] D. Wu, F. Xu, B. Sun, R. Fu, H. He, K. Matyjaszewski, Chem. Rev. 112 (2012) 3959–4015 https://doi.org/10.1021/cr200440z.
[12] C. Gu, N. Huang, J. Gao, F. Xu, Y. Xu, D. Jiang, Angew. Chem. Int. Ed. 53 (2014) 4850–4855 https://doi.org/10.1002/anie.201402141.
[13] P. Kaur, J.T. Hupp, S.T. Nguyen, ACS Catal. 1 (2011) 819–835 https://doi.org/10.1021/cs200131g.
[14] Z.-A. Qiao, S.-H. Chai, K. Nelson, Z.H. Bi, J.H. Chen, S.M. Mahurin, X. Zhu, S. Dai, Nat. Commun. 5 (2014) 3705 https://doi.org/10.1038/ncomms4705.
[15] J.-S.M. Lee, T.-H. Wu, B.M. Alston, M.E. Briggs, T. Hasell, C.-C. Hu, A.I. Cooper, J. Mater. Chem. 4 (2016) 7665–7673 https://doi.org/10.1039/c6ta02319c.
[16] H. Xu, S.S. Tao, D.L. Jiang, Nat. Mater. 15 (2016) 722–726 https://doi.org/10.1038/NMAT4611.
[17] T. Ben, H. Ren, S. Ma, D. Cao, J. Lan, X. Jing, W. Wang, J. Xu, F. Deng, J.M. Simmons, S. Qiu, G. Zhu, Angew. Chem. Int. Ed. 48 (2009) 9457–9460 https://doi.org/10.1002/anie.200904637.
[18] P.M. Budd, B.S. Ghanem, S. Makhseed, N.B. McKeown, K.J. Msayib, C.E. Tattershall, Chem. Commun. (2004) 230–231 https://doi.org/10.1039/B311764B.
[19] J.S. Zhang, Z.-A. Qiao, S.M. Mahurin, X.G. Jiang, S.-H. Chai, H.F. Lu, K. Nelson, S. Dai, Angew. Chem. Int. Ed. 54 (2015) 4582–4586 https://doi.org/10.1002/ange.201500305.
[20] A.P. Côté, A.I. Benin, N.W. Ockwig, M. O'Keeffe, A.J. Matzger, O.M. Yaghi, Science 310 (2005) 1166–1170 https://doi.org/10.1126/science.1120411.
[21] J.X. Jiang, F. Su, A. Trewin, Wood, C.D.N.L. Campbell, H. Niu, C. Dickinson, A.Y. Ganin, M.J. Rosseinsky, Y.Z. Khimyak, A.I. Cooper, Angew. Chem. Int. Ed. 46 (2007) 8574–8578 https://doi.org/10.1002/anie.200701595.
[22] P. Kuhn, M. Antonietti, A. Thomas, Angew. Chem. Int. Ed. 47 (2008) 3450–3453 https://doi.org/10.1002/anie.200705710.
[23] P. Kuhn, A. Forget, D. Su, A. Thomas, M. Antonietti, J. Am. Chem. Soc. 130 (2008) 13333–13337 https://doi.org/10.1021/ja803708s.
[24] J.-X. Jiang, F. Su, A. Trewin, C.D. Wood, H. Niu, J.T.A. Jones, Y.Z. Khimyak, J. Am. Chem. Soc. 130 (2008) 7710–7720 https://doi.org/10.1021/ja8010176.
[25] Y. Yuan, F. Sun, H. Ren, X. Jing, W. Wang, H. Ma, H. Zhao, G.J. Zhu, J. Mater. Chem. 21 (2011) 13498–13502 https://doi.org/10.1039/c1jm11998b.
[26] L.M. Tao, F. Niu, J.G. Liu, T.M. Wang, Q.H. Wang, RSC Adv. 6 (2016) 94365–94372 https://doi.org/10.1039/c6ra21196h.
[27] G. Wang, K. Leus, H.S. Jena, C. Krishnaraj, S. Zhao, H. Depauw, N. Tahir, Y. Liu, P.V.D. Voort, J. Mater. Chem. 6 (2018) 6370–6375 https://doi.org/10.1039/C7TA08913A.
[28] S. Hug, L. Stegbauer, H. Oh, M. Hirscher, B.V. Lotsch, Chem. Mater. 27 (2015) 8001–8010 https://doi.org/10.1021/acs.chemmater.5b03330.
[29] P. Kuhn, A. Thomas, M. Antonietti, Macromolecules 42 (2009) 319–326 https://doi.org/10.1021/ma802322j.
[30] S. Hug, M.B. Mesch, H. Oh, N. Popp, M. Hirscher, J. Senker, B.V. Lotsch, J. Mater. Chem. 2 (2014) 5928–5936 https://doi.org/10.1039/c3ta15417c.
[31] H.P. Ma, H. Ren, S. Meng, F.X. Sun, G.S. Zhu, Sci. Rep. 3 (2013) 2611 https://doi.org/10.1038/srep02611.
[32] M.G. Rabbani, H.M. El-Kaderi, Chem. Mater. 24 (2012) 1511–1517 https://doi.org/10.1021/cm300407h.
[33] M.G. Rabbani, T.E. Reich, R.M. Kassab, K.T. Jackson, H.M. El-Kaderi, Chem. Commun. 48 (2012) 1141–1143 https://doi.org/10.1039/c2cc16986j.
[34] A.K. Sekizkardes, S. Altarawneh, Z. Kahveci, T. İslamoğlu, H.M. El-Kaderi, Macromolecules 47 (2014) 8328–8334 https://doi.org/10.1021/ma502071w.
[35] X.J. Zhang, N. Bian, L. J Mao, Q. Chen, L. Fang, A.D. Qi, B.H. Han, Macromol. Chem. Phys. 213 (2012) 1575–1581 https://doi.org/10.1002/macp.201200074.
[36] L.M. Tao, F. Niu, C. Wang, J.G. Liu, T.M. Wang, Q.H. Wang, J. Mater. Chem. 4 (2016) 11812–11820 https://doi.org/10.1039/c6ta05107c.
[37] C.Y. Gu, D.Y. Liu, W. Huang, J. Liu, R.Q. Yang, Polym. Chem. 6 (2015) 7410–7417 https://doi.org/10.1039/c5py01090j.
[38] S. Wu, S. Gu, A. Zhang, G. Yu, Z. Wang, J. Jian, C. Pan, J. Mater. Chem. 3 (2015) 878–885 https://doi.org/10.1039/c4ta04734f.
[39] K.S.W. Sing, D.H. Everett, R.A.L. Haul, R.A. Moscou, J. Pierotti, T. Rouquerol, Pure Appl. Chem. 57 (1985) 603–619 https://doi.org/10.1351/pac198557040603.

[40] Y. Zhao, K.X. Yao, B. Teng, T. Zhang, Y. Han, Energy Environ. Sci. 6 (2013) 3684–3692 https://doi.org/10.1039/c3ee42548g.
[41] K.Y. Yuan, C. Liu, L.S. Zong, G.P. Yu, S.L. Cheng, J.Y. Wang, Z.H. Weng, X.G. Jian, ACS Appl. Mater. Interfaces 9 (2017) 13201–13212 https://doi.org/10.1039/c3ta13407e.
[42] A. Bhunia, I. Boldog, A. Moller, C. Janiak, J. Mater. Chem. 1 (2013) 14990–14999 https://doi.org/10.1039/c3ta13407e.
[43] A. Bhunia, V. Vasylyeva, C. Janiak, Chem. Commun. 49 (2013) 3961–3963 https://doi.org/10.1039/c3cc41382a.
[44] K. Wang, H. Huang, D. Liu, C. Wang, J. Li, C. Zhong, Environ. Sci. Technol. 50 (2016) 4869–4876 https://doi.org/10.1021/acs.est.6b00425.
[45] X. Zhu, C. Tian, G.M. Veith, C.W. Abney, J. Dehaudt, S. Dai, J. Am. Chem. Soc. 138 (2016) 11497–11500 https://doi.org/10.1021/jacs.6b07644.
[46] T. Ben, C. Pei, D. Zhang, J. Xu, F. Deng, X. Jing, S. Qiu, Energy Environ. Sci. 4 (2011) 3991–3999 https://doi.org/10.1039/c1ee01222c.
[47] M.R. Liebl, J. Senker, Chem. Mater. 25 (2013) 970–980 https://doi.org/10.1021/cm4000894.
[48] R. Dawson, D.J. Adams, A.I. Cooper, Chem. Sci. 2 (2011) 1173–1177 https://doi.org/10.1039/c1sc00100k.
[49] Hao Guang-Ping, Wen-Cui Li, Dan Qian, Guang-Hui Wang, Wei-Ping Zhang, Tao Zhang, Ai-Qin Wang, Ferdi Schüth, Hans-Josef Bongard, and an-Hui Lu, J. Am. Chem. Soc. 133 (2011) 11378–11388 https://doi.org/10.1021/ja203857g.
[50] R. Dawson, E. Stockel, J.R. Holst, D.J. Adams, A.I. Cooper, Energy Environ. Sci. 4 (2011) 4239–4245 https://doi.org/10.1039/c1ee01971f.
[51] Y. Fu, Z.Q. Wang, X.B. Fu, J. Yan, C. Liu, C.Y. Pan, G.P. Yu, J. Mater. Chem. 5 (2017) 21266–21274 https://doi.org/10.1039/C7TA05416E.
[52] C.F. Martin, E. Stockel, R. Clowes, D.J. Adams, A.I. Cooper, J.J. Pis, F. Rubiera, C. Pevida, J. Mater. Chem. 21 (2011) 5475–5483 https://doi.org/10.1039/c0jm03534c.
[53] Y. Liu, S. Wu, G. Wang, G. Yu, J. Guan, C. Pan, Z. Wang, J. Mater. Chem. 2 (2014) 7795–7801 https://doi.org/10.1039/c4ta00298a.
[54] X. Zhang, J. Lu, J. Zhang, Chem. Mater. 26 (2014) 4023–4029 https://doi.org/10.1021/cm501717c.
[55] W.C. Song, X.K. Xu, Q. Chen, Z.Z. Zhuang, X.H. Bu, Polym. Chem. 4 (2013) 4690–4696 https://doi.org/10.1039/c3py00590a.
[56] Y.Z. Cui, Y.C. Liu, J.C. Liu, J.F. Du, Y. Yu, S. W, Z.Q. Liang, J.H. Yu, Polym. Chem. 8 (2017) 4842–4848 https://doi.org/10.1039/c7py00856b.
[57] G. Li, Z. Wang, Macromolecules 46 (2013) 3058–3066 https://doi.org/10.1021/ma400496q.
[58] Y. Zhu, H. Long, W. Zhang, Chem. Mater. 25 (2013) 1630–1635 https://doi.org/10.1021/cm400019f.
[59] A.L. Myers, J.M. Prausnitz, AIChE J. 11 (1965) 121–127 https://doi.org/10.1002/aic.690110125.
[60] S. Dey, A. Bhunia, D. Esquivei, C. Janiak, J. Mater. Chem. 4 (2016) 6259–6263 https://doi.org/10.1039/c6ta00638h.
[61] G.Y. Li, B. Zhang, J. Yan, Z.G. Wang, J. Mater. Chem. 4 (2016) 11453–11461 https://doi.org/10.1039/c6ta04337b.
[62] P. Arab, M.G. Rabbani, A.K. Sekizkardes, T. İslamoğlu, H.M. El-Kaderi, Chem. Mater. 26 (2014) 1385–1392 https://doi.org/10.1021/cm403161e.
[63] R. Krishna, Microporous Mesoporous Mater. 185 (2014) 30–50 https://doi.org/10.1016/j.micromeso.2013.10.026.
[64] R. Krishna, RSC Adv. 5 (2015) 52269–52295 https://doi.org/10.1039/c5ra07830j.
[65] R. Krishna, RSC Adv. 7 (2017) 35724–35737 https://doi.org/10.1039/c7ra07363a.
[66] R. Krishna, Separ. Purif. Technol. 194 (2018) 281–300 https://doi.org/10.1016/j.seppur.2017.11.056.

Preparation of benzodiimidazole-containing covalent triazine frameworks for enhanced selective CO_2 capture and separation

Jianfeng Du[a], Yuanzheng Cui[a], Yuchuan Liu[a], Rajamani Krishna[c], Yue Yu[a], Shun Wang[a], Chenghui Zhang[a], Xiaowei Song[a,*] and Zhiqiang Liang[a,b,*],

[a] State Key Lab of Inorganic Synthesis and Preparative Chemistry, Jilin University, Changchun, 130012, P. R. China.

[b] Key Laboratory of Advanced Materials of Tropical Island Resources, Ministry of Education, College of Materials and Chemical Engineering, Hainan University

[c] Van 't Hoff Institute for Molecular Sciences, University of Amsterdam, Science Park 904, 1098 XH Amsterdam, The Netherlands

E-mail: liangzq@jlu.edu.cn; xiaoweisong@jlu.edu.cn

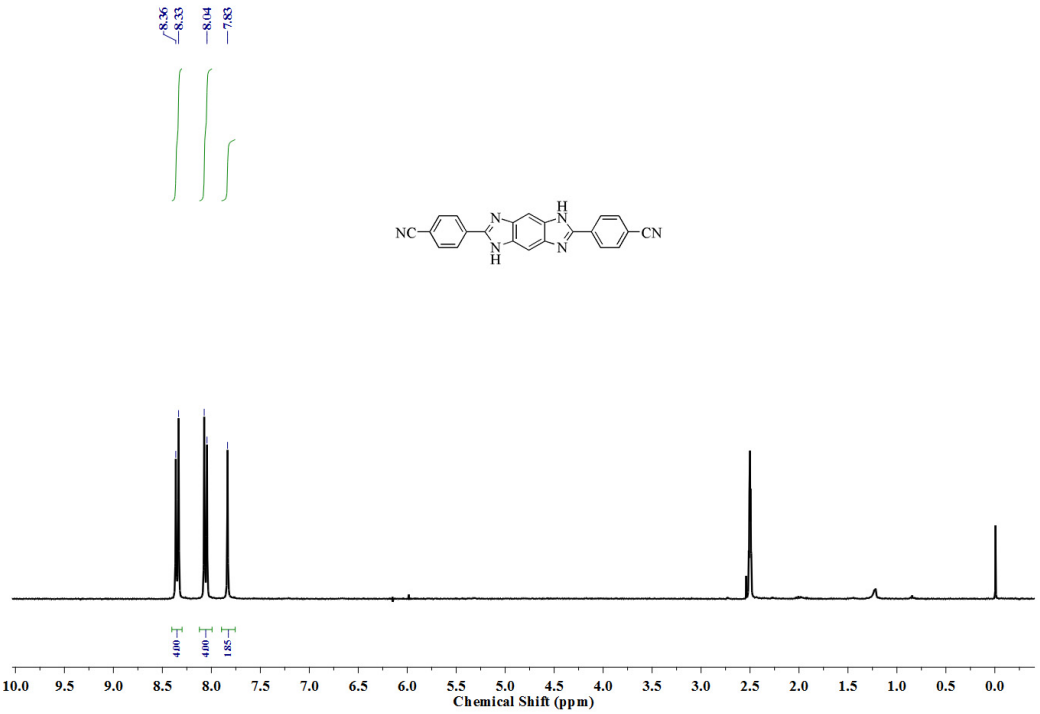

Figure S1. ^{1}H NMR spectrum of **BCBDI**.

Mass Spectrum SmartFormula Report

Analysis Info

Analysis Name C:\Users\Zhonglin\Desktop\data\1\BCBDI_P1-A-4_01_4223.d
Method lc-ms4-hr-low.m
Sample Name BCBDI
Comment

Acquisition D 2017/11/24 15:06:08
Operator zlwei
Instrumen micrOTOF-Q 228888.10351

Acquisition Paramet

Source Type	ESI	Ion Polarity	Positive	Set Nebulizer	0.4 Bar
Focus	Active	Set Capillary	4500 V	Set Dry Heater	200
Scan Begin	50 m/z	Set End Plate	-500 V	Set Dry Gas	5.0 l/min
Scan End	1200 m/z	Set Collision Cell RF	100.0 Vpp	Set Divert Valve	Waste

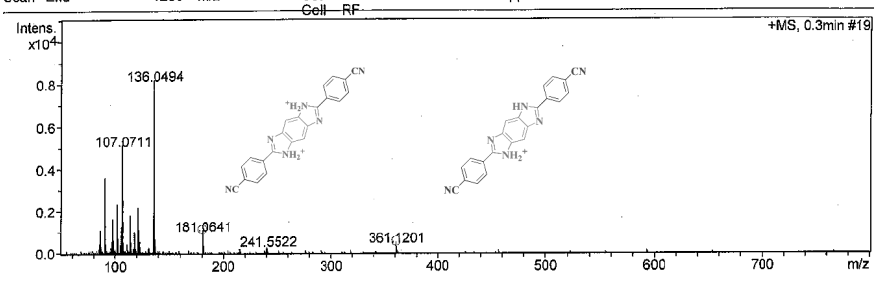

Meas. m/z	#	Ion Formula	m/z	err [ppm]	mSigma	#	mSigma	Score	rdb	e⁻	Con	N-Rule
181.0641	1	C21H18N2O4	181.0628	-7.1	20.5	1		70.85	14.0	even		ok
	2	C17H14N8O2	181.0614	-14.5	21.7	2		25.10	15.0	even		ok
	3	C22H14N6	181.0634	-3.4	21.9	3		100.00	19.0	even		ok
	4	C16H14N10O	181.0671	16.5	22.3	4		17.55	15.0	even		ok
	5	C19H22O7	181.0677	20.3	27.5	5		7.75	9.0	even		ok
	6	C13H10N14	181.0601	-21.9	30.3	6		5.13	16.0	even		ok
	7	C16H18N4O6	181.0608	-18.2	33.8	7		9.93	10.0	even		ok
	8	C26H18O2	181.0648	4.0	34.5	8		69.74	18.0	even		ok
	9	C15H18N6O5	181.0664	12.8	35.0	9		23.64	10.0	even		ok
	10	C11H14N12O3	181.0650	5.4	45.7	10		44.82	11.0	even		ok
	11	C15H22O10	181.0601	-21.9	46.9	11		3.31	5.0	even		ok
	12	C14H22N2O9	181.0657	9.1	48.3	12		27.11	5.0	even		ok
	13	C7H10N18O	181.0637	-2.0	57.8	13		42.34	12.0	even		ok
	14	C10H18N8O7	181.0644	1.7	59.5	14		40.85	6.0	even		ok
	15	C6H14N14O5	181.0630	-5.7	71.6	15		18.41	7.0	even		ok
	16	C9H22N4O11	181.0637	-2.0	73.4	16		24.36	1.0	even		ok
361.1201	1	C26H17O2	361.1223	6.1	67.6	1		50.66	18.5	even		ok
	2	C22H13N6	361.1196	-1.4	78.3	2		100.00	19.5	even		ok
	3	C21H17N2O4	361.1183	-5.1	91.8	3		25.31	14.5	even		ok
	4	C11H13N12O3	361.1228	7.5	131.8	4		1.57	11.5	even		ok
	5	C7H9N18O	361.1201	0.0	144.5	5		4.04	12.5	even		ok
	6	C10H17N8O7	361.1215	3.8	145.5	6		1.89	6.5	even		ok
	7	C6H13N14O5	361.1188	-3.7	158.2	7		0.83	7.5	even		ok
	8	C9H21N4O11	361.1201	0.1	159.3	8		1.51	1.5	even		ok

Figure S2.HR-MS spectrum of **BCBDI.**

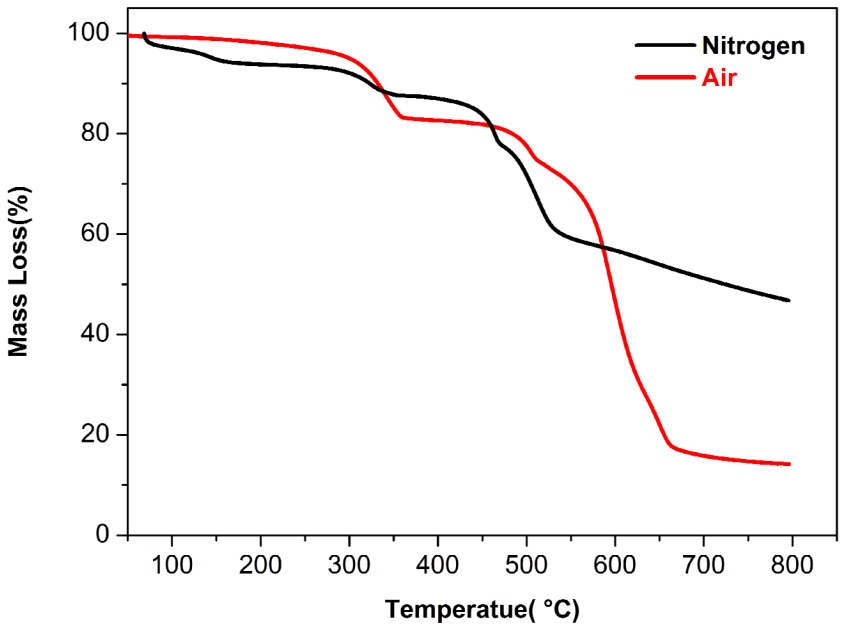

Figure S3. Thermogravimetric analysis (TGA) of **BCBDI** under air (red) and N_2 (black) atmosphere in the range of 35 to 800 ℃ at a heating rate of 10 ℃ min^{-1}.

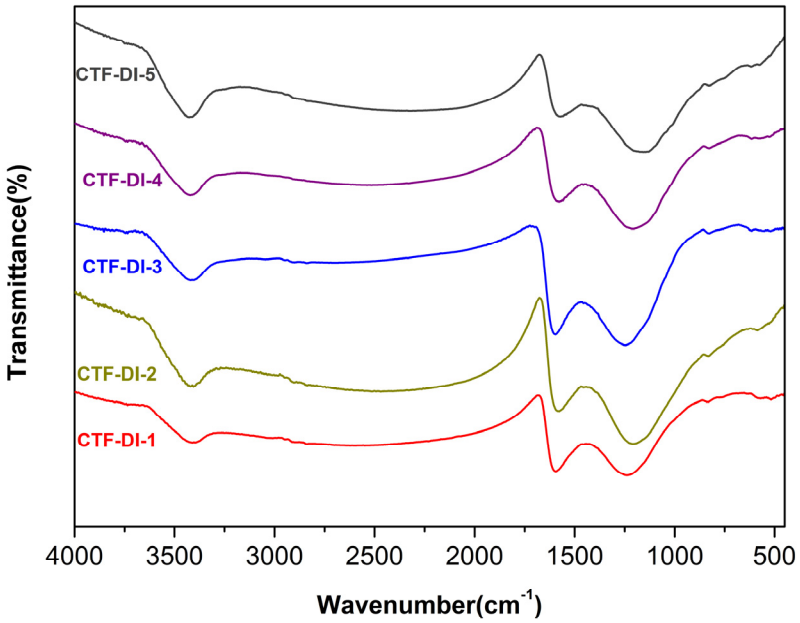

Figure S4. FT-IR spectra of the **CTF-DIs** obtained from different ratios of $ZnCl_2$ to **BCBDI** (KBr pellets).

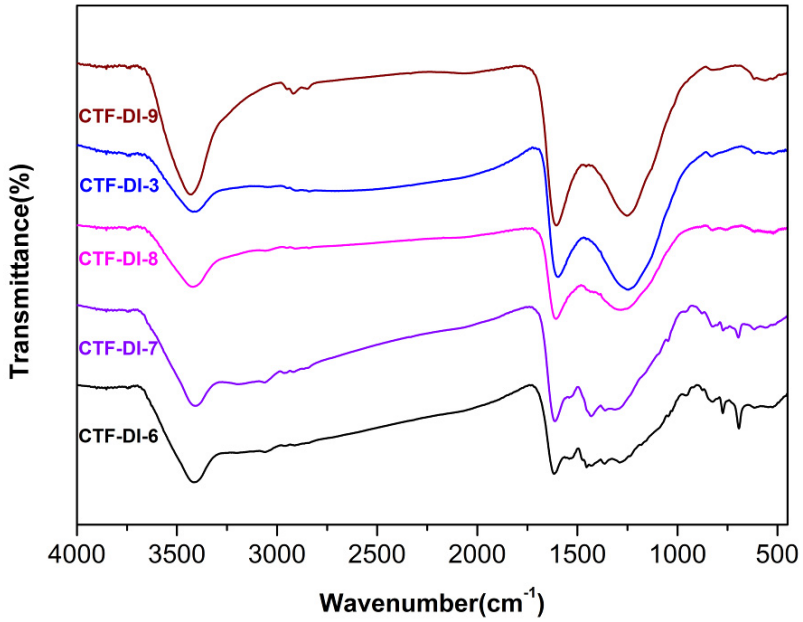

Figure S5. FT-IR spectra of the **CTF-DIs** obtained from different reaction temperatures. (KBr pellets).

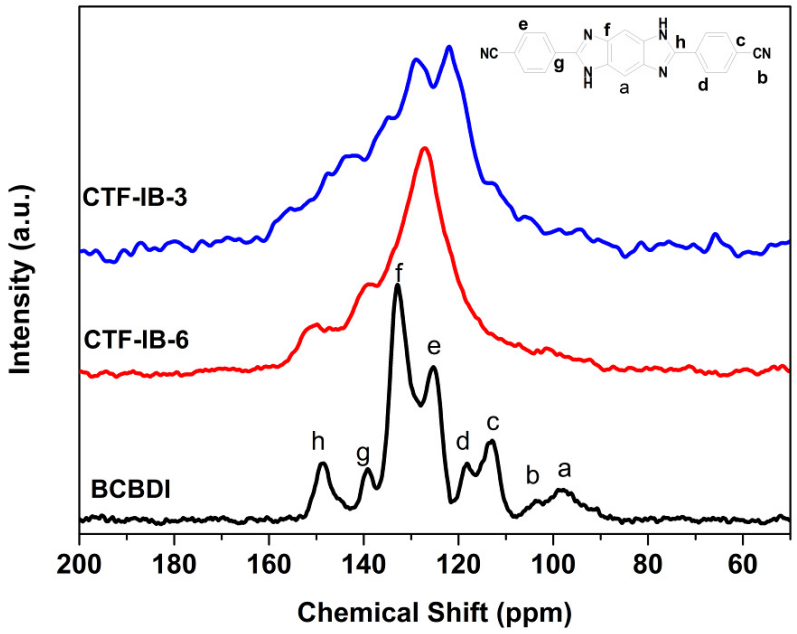

Figure S6. Solid-state ^{13}C CP/MAS NMR Spectra of **CTF-DI-3**, **CTF-DI-6** and **BCBDI.**

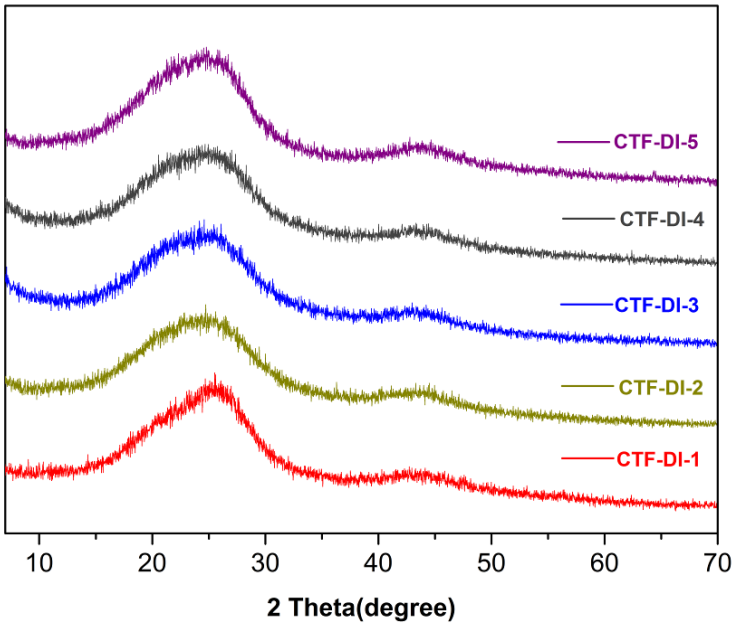

Figure S7. PXRD patterns of **CTF-DI-1–5**.

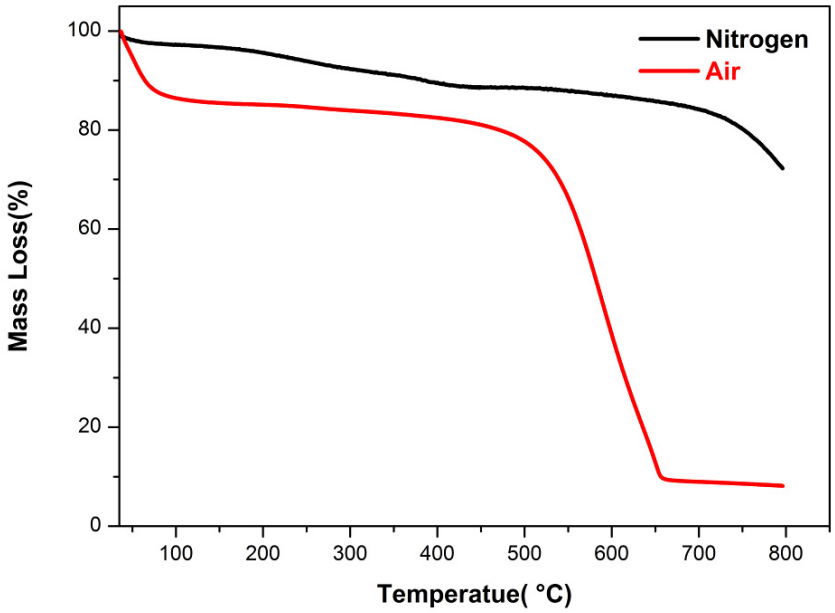

Figure S8. Thermogravimetric analysis (TGA) of **CTF-DI-3** under air (red) and N_2 (black) atmosphere in the range of 35 to 800 °C at a heating rate of 10 °C min^{-1}.

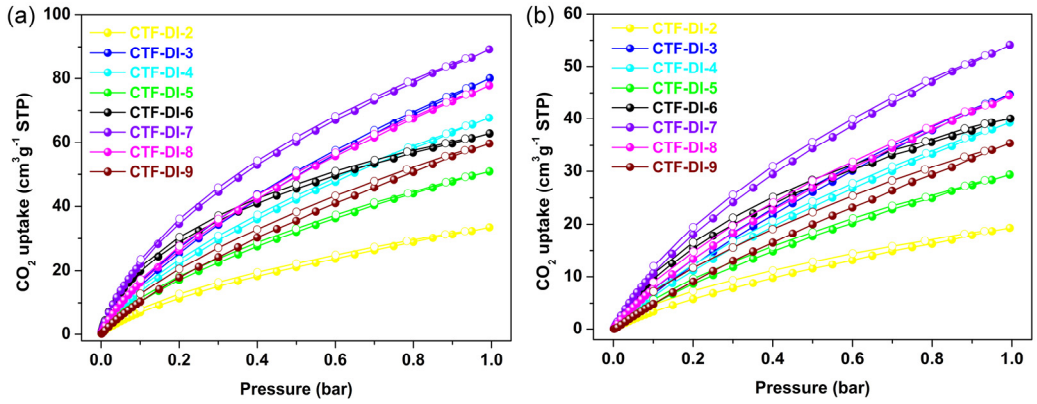

Figure S9. CO_2 adsorption and desorption isotherms at 273 K (a) and 298 K (b) of **CTF-DIs**.

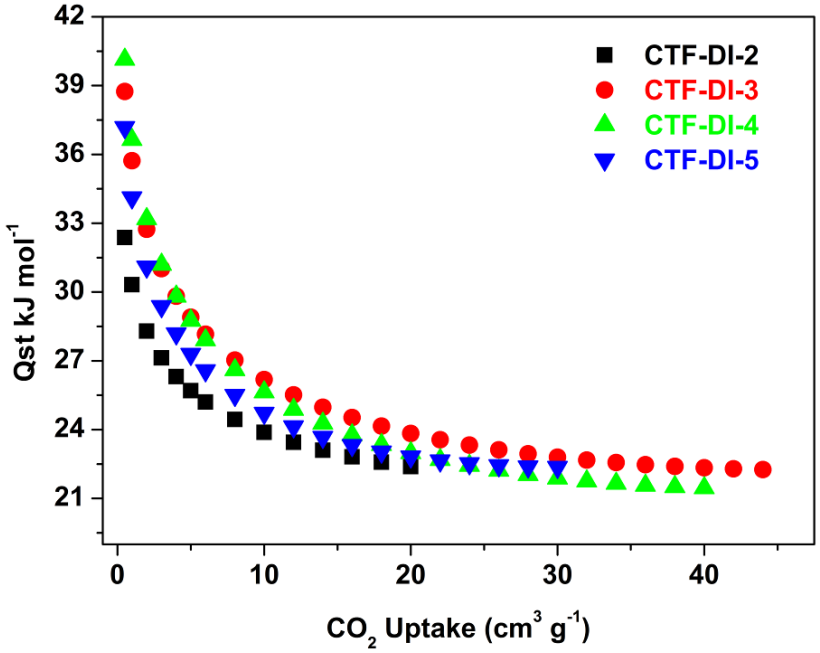

Figure S10. the calculated isosteric heat values of CO_2 adsorption of **CTF-DI-2**–**5**.

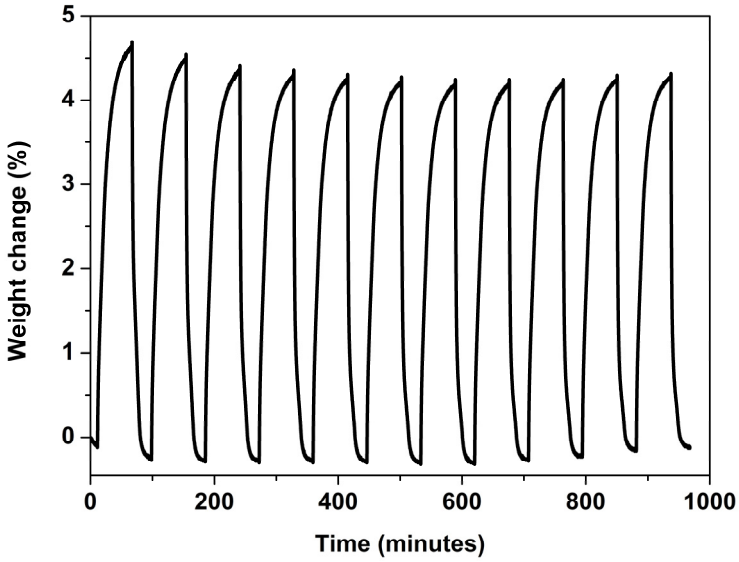

Figure S11. CO_2 adsorption–desorption cycles obtained for **CTF-DI-7** from 25 °C to 80 °C

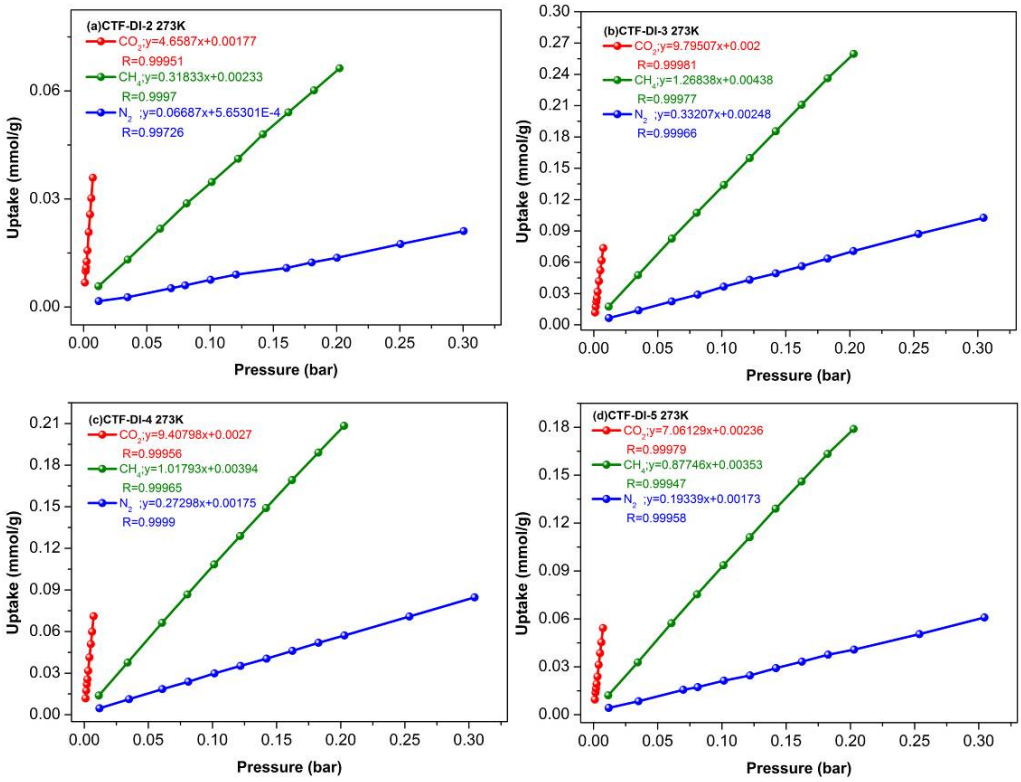

Figure S12. CO_2/N_2 and CO_2/CH_4 initial slope selectivity studies for **CTF-DI-2**–**5**, at 273 K.

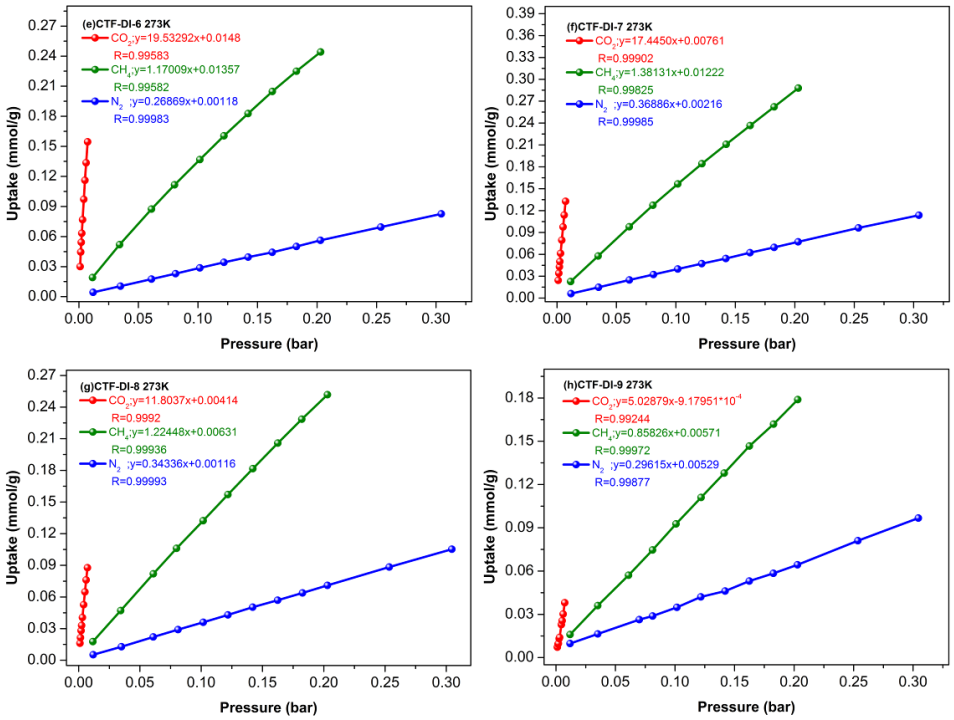

Figure S13. CO_2/N_2 and CO_2/CH_4 initial slope selectivity studies for **CTF-DI-6–9** at 273K.

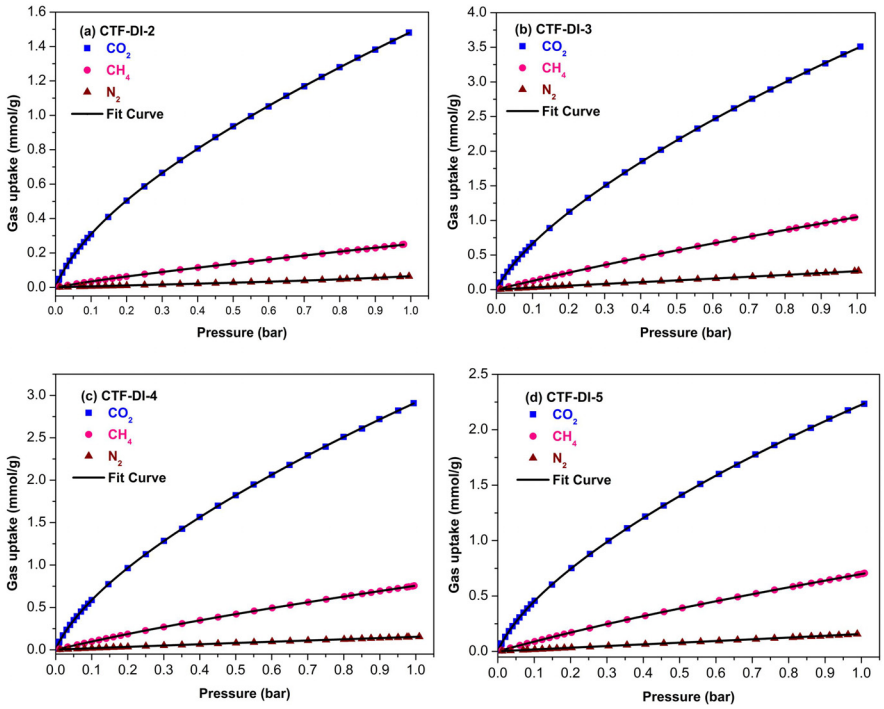

Figure S14. Experimental pure component isotherms for CO_2, CH_4 and N_2 at 273 K and their corresponding dual-site Langmuir-Freundlich curves (solid black lines).

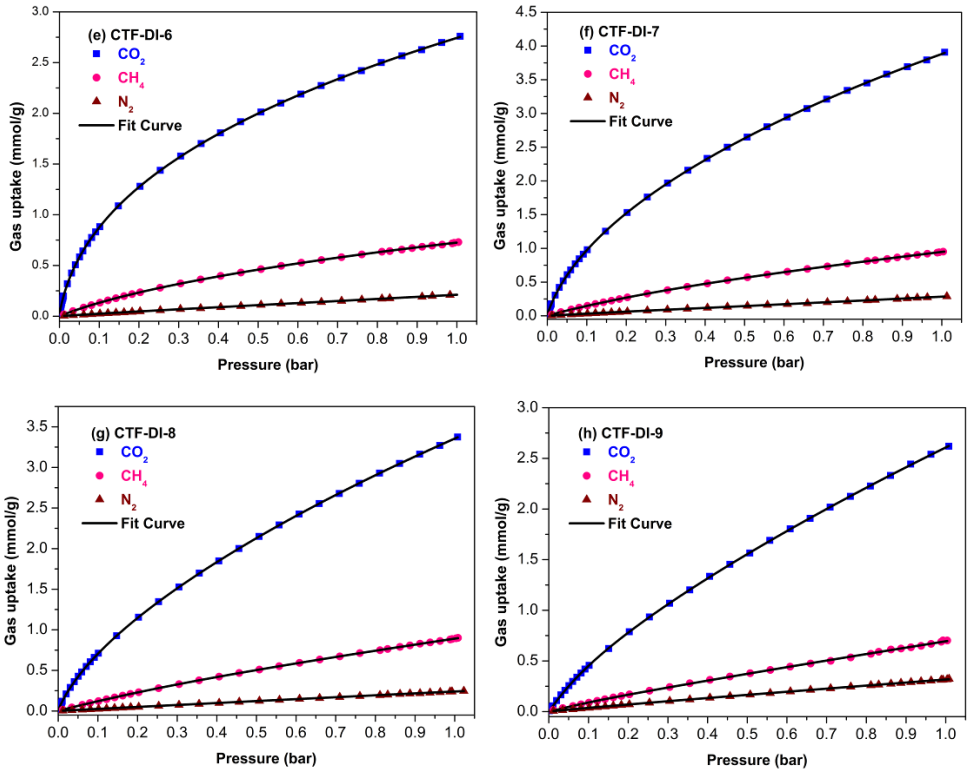

Figure S15. Experimental pure component isotherms for CO_2, CH_4 and N_2 at 273 K and their corresponding dual-site Langmuir-Freundlich curves (solid black lines).

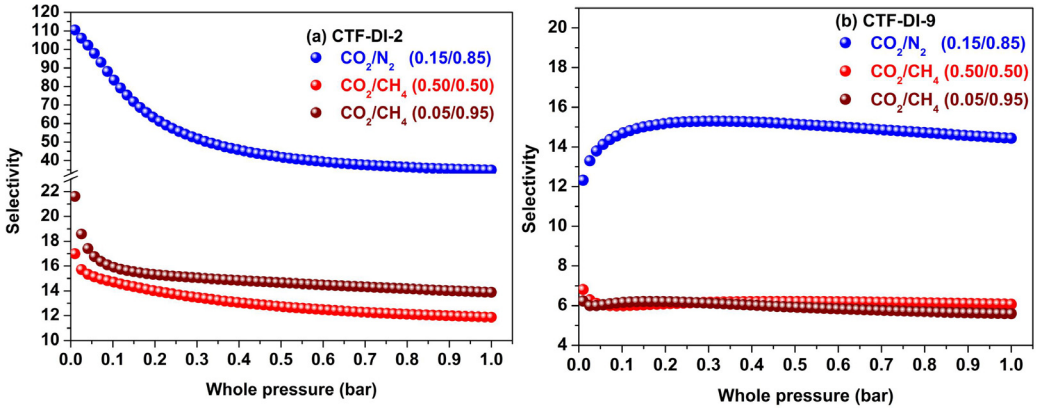

Figure S16. IAST selectivities for the 0.50/0.50 CO_2/CH_4 mixture (red circles), and the 0.05/0.95 CO_2/CH_4 mixture (wine triangles) for **CTF-DI-2** and **CTF-DI-9.**

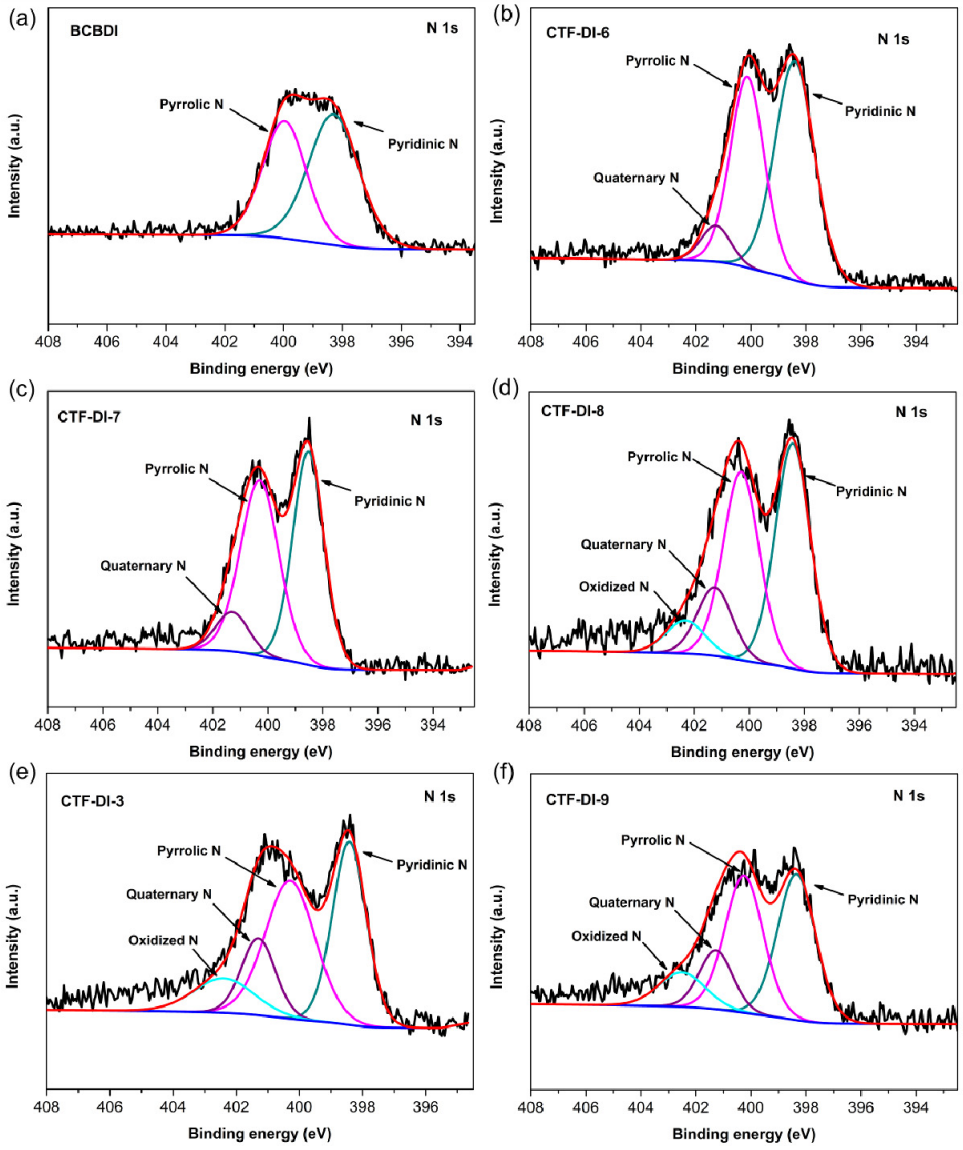

Figure S17. High resolution N 1s XPS spectra of (a) **BCBDI**, (b) **CTF-DI-6** (400 °C), (c) **CTF-DI-7** (450 °C), (d) **CTF-DI-8** (500 °C), (e) **CTF-DI-3** (550 °C), and (f) **CTF-DI-9** (600 °C).

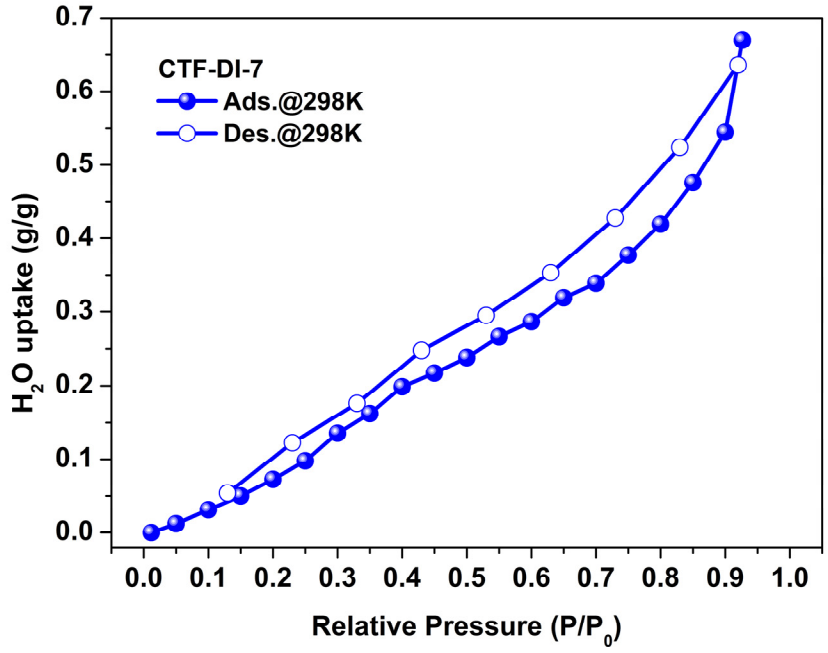

Figure S18. Water vapor sorption isotherms of **CTF-DI-7** at 25 °C.

Calculations of the Isosteric Heats of Gas Adsorption (*Q*st)

The isosteric heat was calculated using the Claussius - Clapeyron equation:

$$\ln P_1 - \ln P_2 = \frac{Qst}{R}\left(\frac{1}{T_2} - \frac{1}{T_1}\right)$$

P_1 : pressure of the adsorption at T_1 = 273 K

P_2 : pressure of the adsorption at T_2 = 298 K

R : gas constant (8.314 kJ mol^{-1})

Q_{st} : isosteric heat which shows the interactions between the gas molecules and the framework

Prediction of adsorption of binary mixture by IAST theory

The measured experimental data is excess loadings (q^{ex}) of the pure components N_2, CH_4 and CO_2 for **CTF-DIs**, which should be converted to absolute loadings (q) firstly.

$$q = q^{ex} + \frac{pV_{pore}}{ZRT}$$

Here Z is the compressibility factor. The Peng-Robinson equation was used to estimate the value of compressibility factor to obtain the absolute loading, while the measure pore volume is also necessary.

The dual-site Langmuir-Freundlich equation[1] is used for fitting the isotherm data at 273 K.

$$q = q_{m1} \times \frac{b_1 \times p^{1/n_1}}{1 + b_1 \times p^{1/n_1}} + q_{m2} \times \frac{b_2 \times p^{1/n_2}}{1 + b_2 \times p^{1/n_2}}$$

Here p is the pressure of the bulk gas at equilibrium with the adsorbed phase (bar), q is the adsorbed amount per mass of adsorbent (mol kg^{-1}), q_{m1} and q_{m2} are the saturation capacities of sites 1 and 2 (mol kg^{-1}), b_1 and b_2 are the affinity coefficients of sites 1 and 2 (1/bar), n_1 and n_2 are the deviations from an ideal homogeneous surface.

The selectivity of preferential adsorption of component 1 over component 2 in a mixture containing 1 and 2, perhaps in the presence of other components too, can be formally defined as

$$S = \frac{q_1/q_2}{p_1/p_2}$$

q_1 and q_2 are the absolute component loadings of the adsorbed phase in the mixture.

These component loadings are also termed the uptake capacities. We calculate the values of q1 and q2 using the Ideal Adsorbed Solution Theory (IAST)[2] of Myers and Prausnitz.

Transient breakthrough of mixtures in fixed bed adsorbers

For the breakthrough simulations, the following parameter values were used: length of packed bed, L = 0.3 m; voidage of packed bed, e = 0.4; superficial gas velocity at inlet, u = 0.04 m/s. The transient breakthrough simulation results are presented in terms of a *dimensionless* time as the x-axis, $\tau = \frac{tu}{L\varepsilon}$, defined by dividing the actual time, t, by the characteristic time, $\frac{L\varepsilon}{u}$. The y-axis is the dimensionless gas concentration, $\frac{c_i}{c_{i0}}$ at the outlet of the fixed bed adsorber.

Notation

b	Langmuir-Freundlich constant, $\mathrm{Pa}^{-\nu}$
c_i	molar concentration of species i in the gas phase, mol m^{-3}
$c_{\mathrm{i}0}$	molar concentration of species i at inlet to adsorber, mol m^{-3}
p_i	partial pressure of species i in mixture, Pa
q	component molar loading of species i, mol kg^{-1}
q_sat	saturation loading, mol kg^{-1}
L	length of packed bed adsorber, m
R	gas constant, 8.314 J mol^{-1} K^{-1}
t	time, s
T	absolute temperature, K
u	superficial gas velocity in packed bed, m s^{-1}

Greek letters

ε voidage of packed bed, dimensionless

v Freundlich exponent, dimensionless

τ time, dimensionless

ρ framework density, kg m^{-3}

Table S1. CO_2 uptake of **CTF-DIs** at 273 K / 0.15 bar and 273 K / 0.50 bar.

Samples	CO_2 uptake (cm^3 g^{-1})	
	273 K / 0.15 bar	273 K / 0.50 bar
CTF-DI-2	9.2	21.1
CTF-DI-3	20.5	49.5
CTF-DI-4	17.7	42.1
CTF-DI-5	13.6	32.1
CTF-DI-6	24.6	45.6
CTF-DI-7	28.3	60.2
CTF-DI-8	21.1	49.3
CTF-DI-9	14.1	35.6

Table S2. Elemental Analysis of the **CTF-DIs**.

Code	N (%)	C (%)	H (%)
Calculated	23.32	73.32	3.360
CTF-DI-6	17.24	61.03	3.016
CTF-DI-7	16.19	63.83	2.922
CTF-DI-8	13.23	69.83	2.377
CTF-DI-3	12.88	69.84	2.517
CTF-DI-6	10.99	51.67	2.757

Table S3. The refined parameters for the Dual-site Langmuir-Freundlich equations fit for the pure isotherms of N_2, CH_4 and CO_2 for **CTF-DIs** at 273 K.

CTF-DIs	Gas	q_{m1}	b_1	$1/n_1$	q_{m2}	b_2	$1/_{n2}$	R^2
CTF-DI-2	**N_2**	0.29725	6.6196E-10	3.95379	2.62982	2.47765E-4	0.94006	0.99931
	CH_4	0.02807	0.0449	1.19488	2.64452	7.58248E-4	1.04276	0.99980
	CO_2	0.41657	0.07369	0.90681	12.17749	0.00155	0.90958	0.99999
CTF-DI-3	**N_2**	4.21725	1.27109E-5	1.71152	0.22618	0.01354	0.99889	0.99972
	CH_4	205.1932	7.07584E-5	0.92131	0.04605	0.001	2.05571	0.99996
	CO_2	0.47314	0.09367	0.96254	17.59275	0.00319	0.91017	0.99999
CTF-DI-4	**N_2**	0.24668	0.00897	0.87092	25.58794	5.21221E-6	1.36378	0.99992
	CH_4	0.09392	0.00514	1.45074	106.0441	9.97852E-5	0.90557	0.99999
	CO_2	0.50089	0.09255	0.90689	19.32555	0.00262	0.87559	0.99999
CTF-DI-5	**N_2**	0.20272	0.00983	0.94324	14.84312	1.85209E-6	1.70393	0.99982
	CH_4	88.20904	1.08296E-4	0.91071	0.08785	0.00522	1.43188	0.99999
	CO_2	9.27124	0.00311	0.94852	0.46148	0.09856	0.9018	0.99999
CTF-DI-6	**N_2**	2.90736	5.73798E-5	1.45204	0.13367	0.01725	0.98861	0.99977
	CH_4	0.16873	0.04305	1.05313	2.18318	0.00366	0.9988	0.99992
	CO_2	7.85012	0.00762	0.79222	1.15039	0.13071	0.80125	0.99999
CTF-DI-7	**N_2**	3.27337	1.54122E-4	1.33296	0.08231	0.03215	1.0395	0.99980
	CH_4	206.6113	8.76398E-5	0.83036	0.13918	0.00627	1.51722	0.99997
	CO_2	13.50744	0.00542	0.85693	1.0885	0.10044	0.87222	0.99999
	N_2	4.79846	4.12072E-4	1.04514	0.01446	0.08818	0.60167	0.99995

CTF-DI-8	**CH_4**	231.8876	5.96663E-5	0.88535	0.0888	0.00499	1.58316	0.99999
	CO_2	18.08266	0.00337	0.87242	0.58438	0.1031	0.89556	0.99999
CTF-DI-9	N_2	5.33848	2.37176E-6	1.15716	0.11396	0.02452	0.88444	0.99996
	CH_4	0.06998	0.04991	1.25525	6.46395	7.17692E-4	1.08785	0.99964
	CO_2	0.45498	0.06571	1.07794	14.87023	0.0017	1.00384	0.99998

Reference

1. D. M. Ruthven, Principles of Adsorption and Adsorption Processes; Wiley: New York, 1984.

2. A. L. Myers, J. M. Prausnitz, *AIChE. J.* 1965, **11**, 121-127.